



Paper sludge saccharification for batch and fed-batch production of bacterial cellulose decorated with magnetite for dye decolorization by experimental design

Ahmed K. Saleh · Ahmed Salama ·
Ahmed S. Badawy · Mohamed A. Diab ·
Hamada El-Gendi

Received: 18 May 2023 / Accepted: 4 October 2023 / Published online: 31 October 2023
© The Author(s) 2023

Abstract Cellulosic wastes represent a great environmental challenge, with potential conversion to product-added value through microbial fermentation. Currently, bacterial cellulose (BC) is considered a promising natural polymer for multiple applications. However, the high production cost challenges its wide application. Hence, the current study evaluated the applicability of paper sludge as a cost-effective medium for both cellulases and BC production. The local isolate *Streptomyces rochei* revealed the highest cellulase production titer (about 3 U/mL) at optimized conditions. For BC production, batch and fed-batch fermentation strategies were evaluated using

enzymatically hydrolyzed paper sludge. The results asserted the advantage of fed-batch fermentation for advanced BC production (3.10 g/L) over batch fermentation (1.06 g/L) under the same cultivation conditions. The developed BC membranes were characterized through different instrumental analyses, which revealed an increase in fiber diameters and crystallinity under fed-batch fermentation. Furthermore, BC/magnetite (BC/Fe₃O₄) nanocomposite was developed by an in-situ approach. The newly developed composite was evaluated for dye removal applications, using methyl orange (MO) as a model. The dye removal conditions were optimized through Box Behnken design (BBD), which indicated maximal MO removal (83.5%) at pH 3.0 and BC/Fe₃O₄ concentration of 0.1 mg/dL after 60 min. Therefore, the current study asserts the good applicability of enzymatically hydrolyzed paper sludge as a medium for cost-effective BC production and the high capacity of BC/magnetite nanocomposite for MO decolorization. The study paves the way for the cost-effective implementation of BC/magnetite nanocomposite for dye removal.

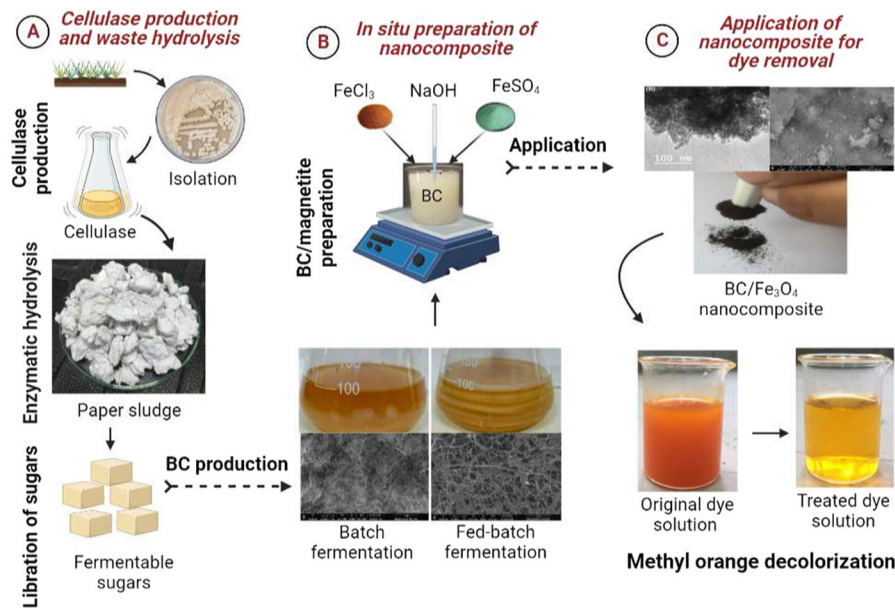
Supplementary Information The online version contains supplementary material available at <https://doi.org/10.1007/s10570-023-05545-6>.

A. K. Saleh (✉) · A. Salama · M. A. Diab
Cellulose and Paper Department, National Research
Centre, El-Tahrir St, Dokki, Giza 12622, Egypt
e-mail: asrk_saleh@yahoo.com

A. S. Badawy
Botany and Microbiology Department, Faculty of Science,
AL-Azhar University, Assiut, Egypt

H. El-Gendi (✉)
Bioprocess Development Department, Genetic
Engineering and Biotechnology Research Institute, City
of Scientific Research and Technological Applications
(SRTA-City), New Borg El-Arab City, Alexandria 21934,
Egypt
e-mail: elgendi1981@yahoo.com

Graphical Abstract



Keywords Bacterial cellulose · Paper sludge · Cellulase production, BC/ Fe_3O_4 nanocomposite · Methyl orange decolorization

Introduction

Cellulosic biomass is a globally abundant waste largely accumulates in the industrial and agricultural sectors. These wastes represent a great environmental challenge facing continuous mass production (Siqueira et al. 2020). For sustainable production, cellulosic wastes could be implemented into several value-added products (Chukwuma et al. 2021; Usmani et al. 2022). Among others, paper sludge is a major solid waste resulting from wood pulping and paper-making processes, with disposal costs representing half of the total paper wastewater treatment (Strezov and Evans 2009; Taramian et al. 2007). Solid paper sludge is usually separated automatically from paper processing machines as a solid with high contents of fine and small cellulosic fiber, kaolin clay, and calcium carbonate (Baziramakenga and Simard 2001; Takizawa et al. 2018). Attributed to its inapplicability for reusing in the paper industry, paper sludge is usually discharged into the environment, representing

a dual challenge for the paper manufacturing and environmental sectors (Turner et al. 2022). Therefore, the valorization of such high cellulosic waste could reduce the treatment cost and environmental threat of the paper industry wastewater. In this regard, several studies reported the direct implementation of paper sludge for pozzolanic material manufacture (García et al. 2008), lactic acid production (Li et al. 2021), ceramic material (Cusidó et al. 2015), and methane production (Takizawa et al. 2018), but the outcome impacts are limited. The utilization of cellulosic biomass for microorganism cultivation is usually limited to the hydrolysis process, which converts the complex cellulose structures into simple fermentable sugars (Dhar et al. 2019; Tripathi et al. 2023a). Sustainable hydrolysis of cellulosic material is usually mediated by microbial cellulases, which have recently increased their market share toward greener and more sustainable biofuel production (Pham et al. 2022). This growing demand for cellulases implies continuous research for potent cellulase-producing isolates with lower production needs (Danso et al. 2022). Beyond enzyme production, BC is a promising natural biopolymer that was recently produced through the hydrolysis of different cellulosic wastes.

The high purity of BC, in addition to its amenability to large-scale production through microbial fermentation, increases its commercial applicability over plant-based cellulose (El-Gendi et al. 2022). Several studies have reported the use of BC in wound dressing, gelling and thickening additives, food packaging, dye removal, and drug delivery polymer, but the production costs limit its widespread and commercial-scale applications (Fatima et al. 2022; Haghghi et al. 2021; Liu et al. 2021). The BC production medium represents about 30% of the total production cost; hence, as a result, greater emphasis has been placed on the cost-effective production of BC from agricultural and industrial wastes (Padmanabhan et al. 2022; Saleh et al. 2021).

It is widely accepted that the normal BC membranes are biologically inactive, though the numerous hydroxyl groups in the BC surface, in addition to its porous structure, provide several sites for biologically active compounds' absorption and loading (Katepetch and Rujiravanit 2011). Hence, regarding the outstanding mechanical properties of BC, increased attention was directed toward its fabrication with diverse biologically active materials for various applications (Sulaeva et al. 2020). An excellent example is the fabrication of nanometals on BC surfaces (Yang et al. 2011). Though several nanometals reveal significant biological activities attributed to their large surface-to-volume ratio, their high tendency to agglomerate and precipitate, especially especially in aqueous solution limited their application. Therefore, their incorporation in BC fibers enhances the particles' stability and even reduces their toxicity by controlling their release (Saleh et al. 2022b).

Pollution with synthetic azo-dyes is currently ranked as one of the growing environmental challenges (Tripathi et al. 2023b; Zhao et al. 2021). Synthetic dyes are heavily implied in the textile, leather, printing, and paper industries, which usually find their way to the water body system as disgorged wastewater (Tamer et al. 2021). These dyes represent a great challenge to the aquatic ecosystem and finally affect human health through drinking water or consumption of contaminated seafood (Yang et al. 2022). Among others, MO (dimethyl amino azo benzenesulfonate) is a widely applied azo dye with significant resistance toward degradation by conventional methods, hence regarded as a model dye for decolorization

studies (Naves et al. 2017; Nguyen et al. 2018; Song et al. 2022). Several approaches are currently being used for waste pollutant removal, but the but the implemented cost and dye removal efficiency remain challenges to current conventional methods (Liu et al. 2021; Yang et al. 2022). In this regard, dye removal through NPs gaining much attention as a low-cost and more efficient alternative (Perwez et al. 2022). In addition to the large surface-to-volume ratio of NPs, the magnetic properties greatly enhanced their repeated implementation in dye absorption applications (Joshi et al. 2019; Kajani and Bordbar 2019). The novelty of the current study is to evaluate the applicability of paper sludge as a waste from the paper industry for sustainable BC production and the effectiveness of the developed BC/Fe₃O₄ nanocomposite for dye removal from industrial wastewater. Therefore, the current study is directed toward the hydrolysis of the paper sludge by cellulase production from a local actinomycete isolate. Additionally, the cellulase hydrolyzed paper sludge was valorized as a low-cost medium for BC production. Finally, the nanocomposite development based on BC and magnetite (Fe₃O₄) by in situ modification was used for MO dye decolorization.

Materials and methods

Materials

Paper sludge was supplied from the Quena Paper Industry Company in Egypt. Methyl orange (85%, MW: 327.33) was supplied from SD Fine-Chem. Sodium nitrate (NaNO₃, M.W. 84.99), Dipotassium hydrogen phosphate K₂HPO₄ (MW: 174.2), Potassium chloride (KCl, MW: 74.55), and Calcium carbonate (CaCO₃, MW: 100.08) were purchased from Merck Company. Glucose, Ferrous sulphate (FeSO₄.6 H₂O), ferric chloride (FeCl₃), Carboxymethyl cellulose (CMC), Congo red (CR), and Ammonia (NH₃) were purchased from Sigma Aldrich Company. Yeast extract, peptone, disodium hydrogen phosphate were supplied from Loba chemie PVT.LTD. Ethanol absolute (MW: 46.07), and citric acid anhydrous (MW: 192.13) were purchased from Fisher Company. All chemicals were of analytical grade and used without any additional purifications. Distilled water was used for the preparation of all experimental solutions.

Isolation and enrichment of soil actinomycetes

In the course of actinomycetes isolation, different garden soil samples were collected and inoculated into the starch-nitrate medium. Firstly, 100 µl of serially diluted soil samples (10 g soil/100 mL of saline) were uniformly streaked on the starch-nitrate medium containing (g/L): soluble starch, 20; NaNO₃, 2; K₂HPO₄, 1; KCl, 0.5; MgSO₄·7H₂O, 0.5; CaCO₃·2H₂O, 2; and agar, 20 (Jensen et al. 1991). The final medium pH was adjusted to 7.0 and supplied with nystatin (25 mg/mL) as an antifungal agent after sterilization. The inoculated plates were incubated at 37 °C for 7 days. The developed actinomycetes colonies were picked out and streaked on the same medium to ensure purity.

Screening of cellulase activity on carboxymethyl cellulose (CMC) plates

All purified isolates were screened for cellulase production on CMC plates through the Congo red (CR) method (Lisdiyanti et al. 2012). Briefly, purified isolates were individually streaked on CMC agar plates and incubated at 37 °C for 7 days. After incubation, the plates were flooded with CR solution (0.1% w/v). After 15 min, the CR solution was discarded, and plates were flooded with 1 M NaCl to remove excess stain. The developing halo-zone around bacterial growth indicated cellulase activity.

Quantitative evaluation of cellulase activity

The isolates revealing cellulase activity on CMC agar were selected and cultivated under shaking flask conditions on CMC broth at 37 °C for 7 days. Then, the cell-free fermentation broth was used as a source for crude cellulase enzyme. The assay was conducted according to the method of (Wang et al. 1988) as follows; 100 µl of cell-free supernatant was added to 200 µl of CMC (0.5%, w/v) dissolved in sodium acetate buffer (pH 6.0) and incubated at 50 °C. After 15 min, 600 µl of 3,5-dinitrosalicylic acid (DNS) reagent was added. The reaction mixture was then boiled for 10 min at 100 °C before being rapidly cooled on ice. The developed color was measured at 540 nm. The cellulase activity was derived from the glucose standard curve, where one unit of CMCase activity is the quantity of enzyme that releases 1 mg of glucose

per min under standard assay conditions (Miller 1959).

Morphological and molecular identification

Several morphological and biochemical characteristics of the most potent cellulase-producing isolate were evaluated according to Shirling and Gottlieb (Shirling and Gottlieb 1966) as a preliminary identification. Furthermore, the isolate's mycelium and spore morphology were evaluated through scanning electron microscopy (SEM) using a JEOLTM JSM 5400 LV, (Japan) scanning electron microscope at 15–20 kV.

The preliminary identification of the MAE isolate was confirmed at the molecular level through 16S rRNA sequencing. First, the total DNA was isolated according to the manufacturing instructions of the Wizard Genomic DNA Isolation Kit (Promega, USA). After DNA purification, the 16S rRNA gene was retrieved from total purified DNA through a polymerase chain reaction (PCR) using the following universal primers: 27F (5-AGAGTTTGATCMTGGCTCAG-3) and reverse primer 1492R (5-GGTTACCTTGTTACGACTT-3). The PCR product was purified through a purification kit (QIAGEN, Hilden, Germany), where the 16S rRNA gene integrity and purity were evaluated through a 1% agarose gel and spectrophotometry at a UV range (260/280 nm ratio), respectively. The purified PCR product was sequenced according to chain termination techniques through a Genetic Analyzer system (3130XL, Bedford, MA, USA). The BLAST tool was applied to align the 16S rRNA gene of the MAE isolate to the homologs gene sequences in the GenBank database through multiple sequence alignments. The phylogenetic relationship of the selected local isolate to relative organisms was also elucidated through MEGA 5 software based on the 16S rRNA sequence.

Optimization of culture conditions for cellulase production

About six cellulase production media were screened to determine the optimum nutritional factors for maximal cellulase production from MAE isolate, as illustrated in Table S1. In this regard, the isolate MAE was cultivated on different broth media and incubated at 37 °C for 7 days. The effect of pH on cellulase

production was determined by cultivating the MAE isolate on the selected culture medium at pH values of 4, 5, 6, 7, 8, 9, and 10. The flasks were incubated at 37 °C for 7 days. Accordingly, the optimum incubation temperature for cellulase production was also evaluated at different temperatures of 30, 35, 40, 45, 50, and 55 °C. To evaluate the applicability of paper sludge for cellulase production, the CMC content (10 g/L) in the M5 medium was replaced with paper sludge (10 g/L) and cellulase production was evaluated under optimum conditions for 8 days. All flasks were incubated at the recommended conditions of previous experiments with shaking of 160 rpm. The cellulase activity (U/mL) was evaluated in the cell-free supernatant, where corresponding cell growth (g/L) in M5 medium was measured after culture centrifugation (11,000 rpm for 10 min) and drying to a constant weight. The results represented are the average values of triplicate experiments.

Enzymatic hydrolysis of paper sludge

The paper sludge waste was subjected to enzymatic hydrolysis (through cellulase) to maximize its content of fermentable sugars. About 25 g of air-dried paper sludge was initially dispersed in 100 mL of 50 mM acetate buffer (pH 4.7) using a high-speed blender (800ES blender, 230 V, 50 HZ, 330 W, model BB90E, USA) for 20 min. The obtained homogenate was then hydrolyzed through 1 g of freeze-dried cellulase from the MAE isolate (450 U/g) at 50 °C for 84 h at 100 rpm. The paper sludge hydrolysis was monitored by measuring glucose, reducing sugars, and total carbohydrates using the glucose detection kit (Oxidase) (Saleh et al. 2022a), DNS method (Miller 1959), and anthrone-sulfuric acid method (Ludwig and Goldberg 1956), respectively. The enzymatic hydrolysis rate (Ibrahim et al. 2011) of paper sludge was evaluated according to the following equation:

$$\text{Enzymatic hydrolysis rate} = \left[\frac{\text{glucose concentration (g/L)}}{\text{time (h)}} \right] \times 100 \quad (1)$$

BC production under batch and fed-batch fermentation

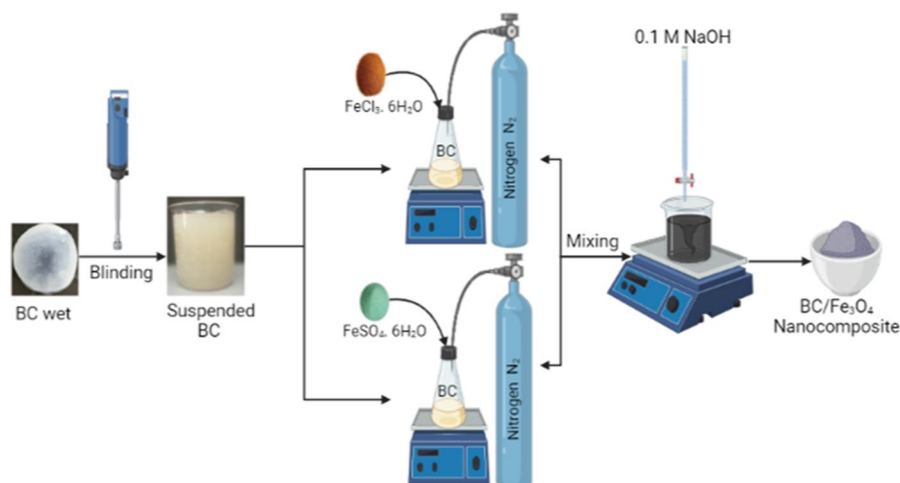
Lactiplantibacillus plantarum AS.6 (*L. plantarum* AS.6) used in this study was isolated from rotten

apples with significant BC production potential, as reported in our previous work (Saleh et al. 2022c). The stock culture was maintained on Hestrin and Schramm's (HS) agar slants, transferred, and stored at 4 °C until used. One loop of inoculum from the agar plate was cultured in a 250 mL conical flask containing 50 mL of HS media composed of 2% glucose, 0.5% yeast extract, 0.5% peptone, 0.27% disodium hydrogen phosphate, 0.115% citric acid, 0.5% ethanol at pH 5.5 and incubated at 30 °C for 2 days under shaking of 200 rpm (Hestrin and Schramm 1954). Two different fermentation strategies were used for BC production: batch and fed-batch fermentation. For batch fermentation, three different preparations media were used for BC production: HS as standard medium, and enzymatic hydrolysate of paper sludge media supplemented with or without glucose-free HS medium (coded as EHPS/HS, and EHPS, respectively). The 250 mL Erlenmeyer flask containing 100 mL of each medium was adjusted to pH 5.5, inoculated with 10% *L. plantarum* AS.6 and incubated under static at 30 °C for 15 days. The fed-batch fermentation was carried out according to (Shezad et al. 2010) with little modification, the same above-mentioned media were used but the 250 mL Erlenmeyer flask containing 50 mL of media was incubated at the same conditions with feeding the media with 5 mL of fresh media every 3 days under aseptic conditions. To purify BC, first the BC membranes were separated from the culture broth. All of the BC membranes were treated with 0.5% NaOH for 30 min at 90 °C, to release trapped medium and bacterial cells. The BC membranes were rinsed extensively with distilled water (ddH₂O) until the pH of the ddH₂O became neutral. The purified BC membranes were dried in an oven at 70 °C to a constant weight and then weighed (Hsieh et al. 2016). The experiment was carried out in triplicate. The production, yield, and productivity of BC were investigated as parameters of BC production (Khan et al. 2020). The BC production (g/L) was calculated based on the total BC amount (dry weight) and the volume of the production media g/L,

$$\text{Yield of BC \%} = \frac{\text{BC (g/L)}}{\text{Original sugar (g/L)}} \times 100 \quad (2)$$

$$\text{Productivity of BC \%} = \frac{\text{BC (g/L)}}{\text{Production time (day)}} \times 100 \quad (3)$$

Fig. 1 Schematic representation illustrating the in situ BC/Fe₃O₄ nanocomposite preparation



In situ development of BC/Fe₃O₄ nanocomposite

In this experiment, an in situ chemical co-precipitation approach was employed to synthesize BC/Fe₃O₄ nanocomposite according to (Salama et al. 2018) with little modifications. As shown in Fig. 1, the wet BC membrane (50 g) was dispersed in 100 mL of ddH₂O by a high-speed blender (800ES blender, USA) for 15 min to form BC slurry (Solution A). In a 250 mL flask, about 5.2 g of ferric chloride (FeCl₃·6 H₂O) were dissolved in 30 mL of BC slurry (Solution B). Also, 2.674 g of ferrous sulphate (FeSO₄·6 H₂O) were dissolved in 30 mL of BC slurry (Solution C). Both solutions B and C were vigorously stirred for 2 h at 60 °C and deoxygenated using an N₂ atmosphere to remove air and create an oxygen-free condition during the synthesis process. They were then mixed and deoxygenated again for 30 min. Finally, 0.1 M NaOH was added dropwise into the reaction mixture until the pH reached around 10, at which point the mixture turned black, indicating the deposit of Fe₃O₄-NPs on BC. The resultant black residue was filtered and washed several times with ddH₂O until it was neutral. The BC/Fe₃O₄ nanocomposite was then freeze-dried and stored until used. The BC/Fe₃O₄ nanocomposite was tested using a magnetic bar (Fig. S1).

Characterization of BC samples and BC/Fe₃O₄ nanocomposite

The surface morphology of BC samples and BC/Fe₃O₄ nanocomposite was evaluated through a

Hitachi S-4800 scanning electron microscope (SEM). The fibers diameter and pore size were determined from different SEM images using the angle tool of ImageJ with Java 1.8.0 software (National Institute of Health (NIH), USA). The average nanofibers diameter and pore size of BC membranes were calculated by measuring around 50–100 points per sample (Wang et al. 2021a). The attenuated total reflectance Fourier Transform Infrared (ATR FT-IR) spectra of the BC samples and BC/Fe₃O₄ nanocomposite were measured in the range of 500 to 4000 cm⁻¹ (FT-IR, 8400s Shimadzu, Japan). X-ray diffraction (XRD) patterns were recorded with an Empyrean Powder Diffractometer (Cu Kα, 0.154 nm) between 5 and 70° 2θ with a step size of 0.01°/s to determine the crystallinity of all samples used. The crystallinity index (CI) values of the samples were calculated according to Segal et al. (1959) using the following equation:

$$CI(\%) = \frac{I_{200} - I_{am}}{I_{200}} \times 100 \quad (4)$$

wherein I_{200} is the intensity of the diffraction peak of (200) lattice plane, and I_{am} is the minimum in intensity between the 010 and 110 peaks at about 18.6°. The transmission electron microscope (TEM) image for BC/Fe₃O₄ nanocomposite was recorded with a JEOL JEM-2100 electron microscope at 100kX magnification, with an acceleration voltage of 120 kV.

Experimental design for MO decolorization

The response surface methodology (RSM) based on the Box-Behnken design (BBD) was employed to identify the optimal level and mutual interaction of the selected parameters for MO decolorization (Box and Behnken 1960). In this experiment, three parameters were evaluated, including medium pH, BC/Fe₃O₄ nanocomposite concentration, and MO removal time. According to the BBD instructions, each parameter was applied at three different levels coded (−1, 0, and +1), which represent the lower, middle, and highest levels of the variable (Table S2). The design matrix included thirteen different experiments (trials), in addition to two identical trials to assess the results' accuracy, whereas the MO decolorization was recorded for each trial as the design response. All trials were prepared in triplicate in a final volume of 100 mL and incubated under shaking (200 rpm) at 30 °C. Process optimization through BBD involves three sequential steps: conducting the optimization experiments according to the design matrix, fitting and analyzing the data, and finally confirming the expected results (Saleh et al. 2020). Hence, in the second step, the measured responses (MO decolorization results) were fitted by regression to a predictive quadratic polynomial model for three parameters:

$$Y = A_0 + B_1(X_1) + B_2(X_2) + B_3(X_3) + B_{12}(X_1X_2) + B_{13}(X_1X_3) + B_{23}(X_2X_3) + B_{11}(X_1)^2 + B_{22}(X_2)^2 + B_{33}(X_3)^2 \quad (5)$$

where Y is the predicted response (MO decolorization), A_0 is a coefficient constant, B_1 , B_2 , and B_3 are linear coefficients, X_1 , X_2 , and X_3 are the three studied variables, B_{12} , B_{13} , and B_{23} are cross-product coefficients, and B_{11} , B_{22} , and B_{33} are quadratic coefficients. The previous model (Eq. 4) was analyzed through analysis of variance (ANOVA) and regression analysis using the JMP IN software, whereas the optimum levels of each variable were predicted for maximum MO decolorization. Additionally, the variables interactions were elucidated in the form of three-dimensional (3D) graphs created through STATISICA 7 software. Each graph represents the effect of interaction of two of the experiment variables upon MO decolorization, when the third variable is constant at its middle value. In the final step of the BBD, the expected optimum levels for each variable were

validated in the laboratory by conducting MO decolorization experiments under the expected optimum levels to evaluate the design model's accuracy. The results represented are the average values of triplicate experiments.

Evaluation of MO decolorization

For evaluating the MO decolorization, the BC/Fe₃O₄ nanocomposite was initially excluded from the MO dye solution by centrifugation at 10,000 rpm for 15 min. The degree of MO decolorization was measured using UV–Vis spectroscopy at 464 nm as follows:

$$\text{MO decolorization} = (D_i - D_f) / D_i \times 100 \quad (6)$$

where D_i and D_f are the initial and final MO concentrations (mg/L), respectively according to (Surip et al. 2020).

Kinetic adsorption study of MO dye

The adsorption study of MO was carried out according to (Surip et al. 2020) with minor modifications. The effect of initial MO concentrations (50 and 150 ppm) upon BC/Fe₃O₄ nanocomposite dye removal capacity was evaluated at the optimum MO decolorization conditions deduced from the BBD experiments. The adsorption capacity of BC/Fe₃O₄ nanocomposite towards MO dye at equilibrium, q_e (mg/g), is calculated as follows:

$$q_e = \frac{(C_i - C_f)V}{W} \quad (7)$$

where C_i and C_f are the initial and final concentrations of the MO dye (mg/L), respectively; where V is the volume of the MO dye solution (mL), while W is the weight of the BC/Fe₃O₄ nanocomposite (mg).

Data analysis

The data of MO decolorization was subjected to multiple-linear regressions using MS Excel 2007 to estimate t value, p value, and confidence levels. The significance level (p value) was determined using the Student's t test. Additionally, the isolate's spore size and fiber diameters of different BC membranes were evaluated through ImageJ software.

Results and discussions

Isolation and screening for cellulase-producing isolates

Several soil samples were screened for cellulase-producing isolates through CMC hydrolysis using the CR staining method. About 19 morphologically different colonies were selected and purified during the actinomycetes isolation course. All retrieved isolates were subjected to cellulase screening on CMC agar plates, where about 10 (out of 19) revealed CMC hydrolysis ability. The quantitative evaluation for CMC hydrolysis activity indicated that isolate-coded MAE showed the highest cellulase activity of about 2.1 U/mL. The

results agree with several studies that reported the high capacity of actinomycetes species for complete cellulose degradation through a group of extracellular cellulose-degrading enzymes (Danso et al. 2022; Daquioag and Penuliar 2021). The isolate MAE was selected, identified, and applied for cellulase production in the following experiments.

Morphological and molecular identification of the MAE isolate

The isolate MAE, which revealed the highest cellulase production, was evaluated for several morphological and biochemical characteristics. As illustrated in Fig. S2, the mature sporulated organism

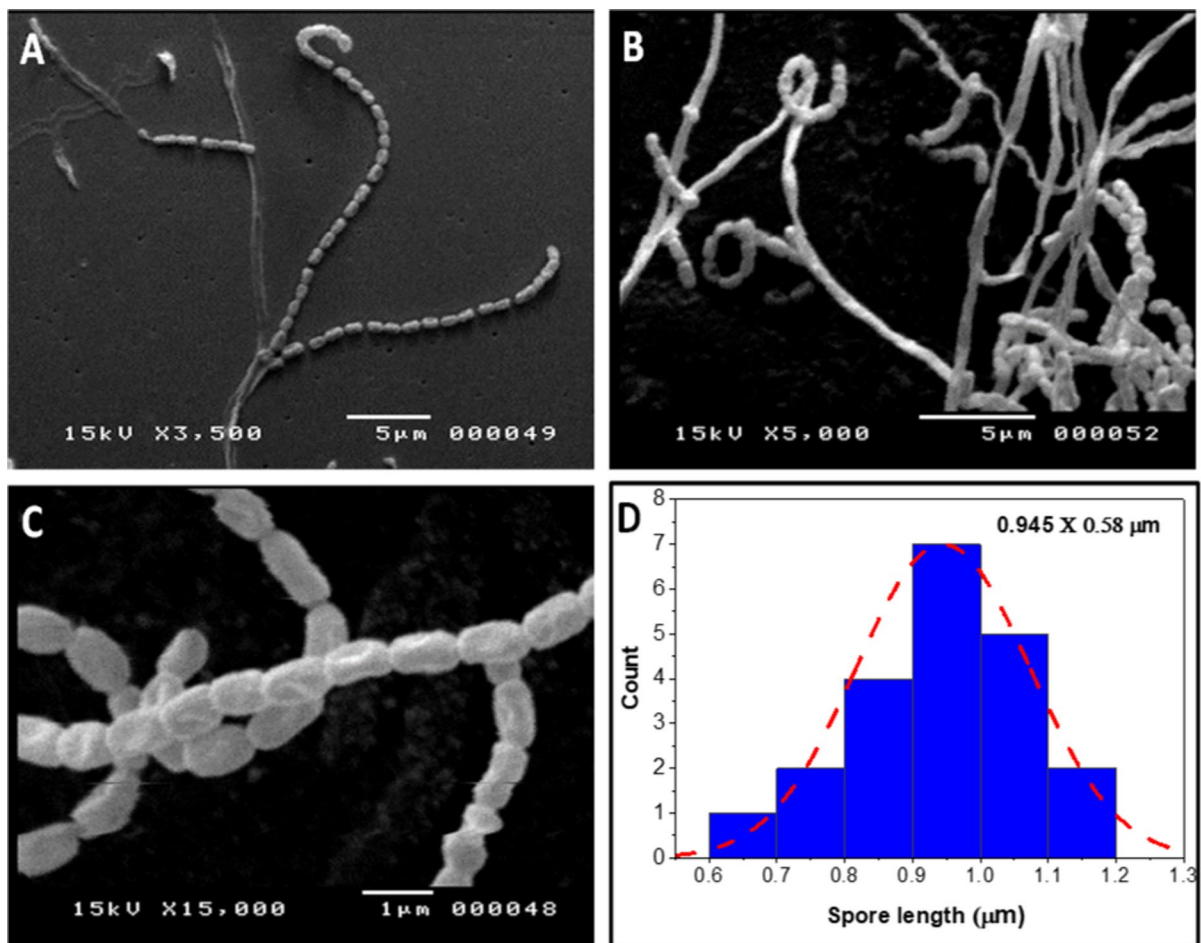


Fig. 2 The morphological structure of the MAE isolate representing the mycelium and spore chains as indicated through scanning electron microscopy (SEM) at magnifications of

3500X (A), 5000X (B), and 15000X (C), with spore dimensions (D) as deduced through ImageJ software

revealed a light brown color with well-developed and abundant substrate and aerial mycelia that characterize members of *Streptomyces* sp. As shown in Table S3, the MAE isolate was identified based on physiological and chemical characteristics including growth conditions, tolerance to growth inhibitors, enzymes profile, nitrogen and carbon sources utilization. This may be attributed to its significant enzyme production potentials, including amylase, protease, pectinase, and chitinase, which are well-reported by several actinomycetes (Javed et al. 2021). The isolate MAE also revealed a significant ability to grow at extreme cultivation conditions of 60 °C and pH 12 and to tolerate many growth inhibitors such as phenol and sodium azide (Otani et al. 2022). The morphological features of the MAE isolate were evaluated through scanning electron microscopy (SEM) as illustrated in Fig. 2.

The results revealed non-fragmented mycelium with globose to rod-shaped spore chains. The spore revealed smooth surfaces with dimensions of about $0.945 \times 0.58 \mu\text{m}$ (length to width).

In the same regard, isolate MAE was identified on the molecular level using 16S RNA gene sequencing. The BLAST results indicated close relatedness of the MAE local isolate to *Streptomyces* sp in the GenBank database with sequence homology of about 97.71% to *Streptomyces rochei*, hence the MAE isolate was deposited in the GenBank under name of *Streptomyces rochei* strain MAE under accession number of OQ175018. The phylogenetic relation of the MAE to other *Streptomyces* was elucidated through the neighbor-joining algorithm of MEGA11 software based upon the bootstrap approach, which confirmed the close

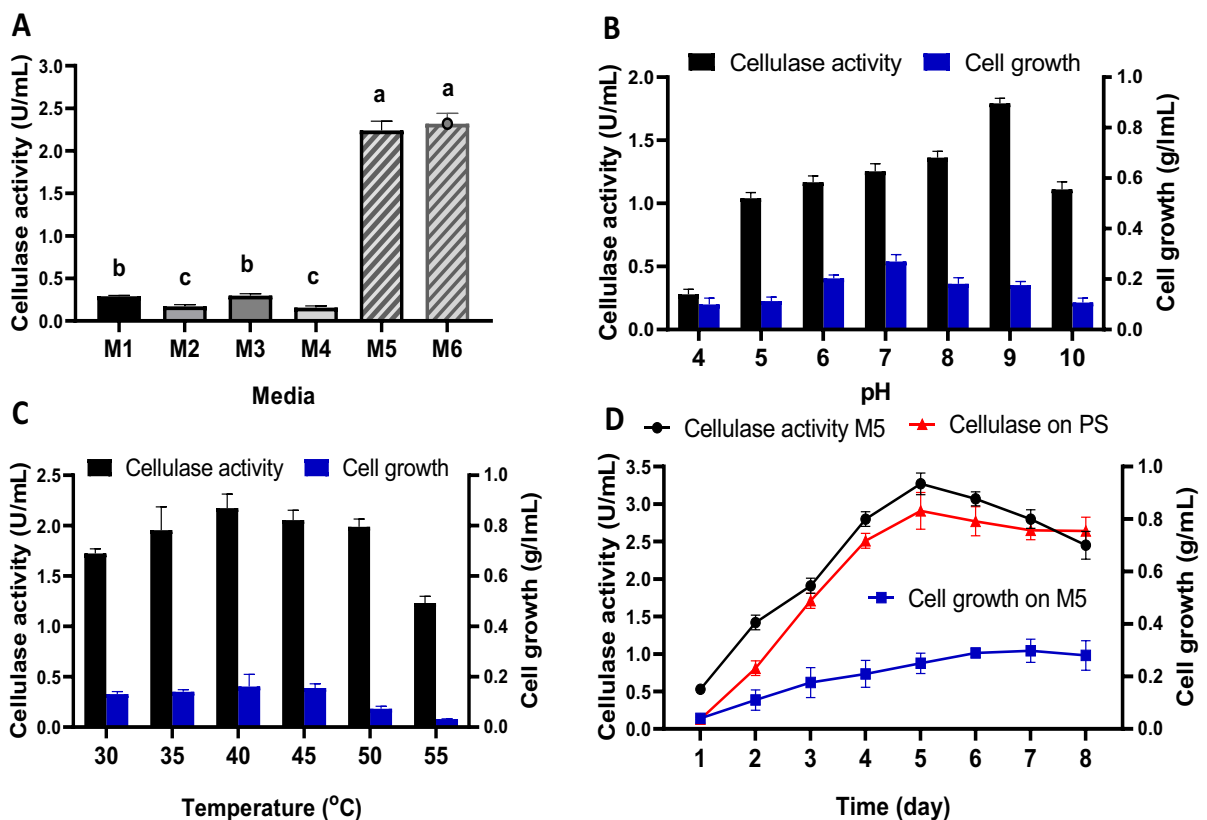


Fig. 3 Effect of different media (A), media pH (B), cultivation temperature (C), and paper sludge (PS) as a source of cellulose compared to M5 medium (D), upon cellulase production and cell growth by *Streptomyces rochei*. The statistical signifi-

cance was calculated through ANOVA of CoStat software at p value ≤ 0.05 using the least significant difference test where the significance of $a > b > c$

relatedness of the MAE isolate to *Streptomyces rochei* (Figure S3).

Optimization of culture conditions for cellulase production

Cellulase production titer is significantly influenced by the production strain and production conditions. Accordingly, the one variable at a time (OVAT) technique was applied to evaluate the following parameters: media composition, media pH, cultivation temperature, and incubation periods to implement the highest production of cellulase as illustrated in Fig. 3. For the quantitative estimation of cellulase enzymes, the selected cellulose-degrading actinomycetes isolates *Streptomyces rochei* was grown in six different broth media. The results represented in Fig. 3A, indicated variation in the cellulase activity titer attributed to medium composition, which ranged from 0.156 to 2.32 U/mL. The results revealed that the maximum cellulase activity was obtained in M6 (2.32 ± 0.12 U/mL), followed by M5 (2.24 ± 0.11 U/mL), whereas M4 represented a low activity of cellulase (0.156 ± 0.02 U/mL). As the difference in the cellulase production between M6 and M5 (about 0.08 U/mL) was insignificant and M6 contains gelatin in its composition, hence M5 was selected for cellulase production as a more affordable and cost-effective medium. Several studies evaluate media compositions for cellulase production and reported 3.69-folds and 1.61-folds increases in cellulase production from *Trichoderma reesei* (Ahamed and Vermette 2009), whereas cellulase activity from *Penicillium brasilianum* KUEB15 was increased about 1.61 fold after media composition optimized (Jung et al. 2015).

Different pH values were evaluated regarding their effect on cellulase production and cell growth (Fig. 3B) from *Streptomyces rochei* isolate. The results indicated the significant effect of medium pH on cellulase production by *Streptomyces rochei*. We can observe that with increased pH, the cellulase production proportionally increased from 0.28 U/mL at pH 4 to a maximum of 1.8 U/mL at pH 9. On the contrary, at a pH higher than 9, the cellulase production was reduced to about 1.1 U/mL. The effect of medium pH on cell growth was slightly different from the cellulase production pattern. The maximum cell mass was reported at pH 7 about 0.27 g/mL,

where cellulase production was about 1.3 U/mL at the same pH value. The pH values below or over 7, adversely affected cell mass formation. The optimum pH for cellulase production is a strain-dependent trait (Mokale Kognou et al. 2022). However, the alkaline optimum pH for cellulase production from *Streptomyces rochei* isolate is in line with another study (Nathan et al. 2014). Regarding the effect of temperature on cellulase production, the results illustrated in Fig. 3C, revealed enhanced cellulase and cell mass production with temperature increasing from 30 to 40 °C. The maximum cellulase and cell mass productions were 2.2 U/mL and 0.16 g/mL, respectively at an incubation temperature of 40 °C. Increasing the temperature over 40 °C, decreased both the cellulase and cell mass production, whereas at 55 °C about 1.2 U/mL and 0.03 g/L, for cellulase and cell mass were detected, respectively. Several studies reported an optimum temperature for cellulase production of about 40 °C, (Fatokun et al. 2016; Saratale et al. 2012) which is in line with the current results.

Furthermore, the CMC content in M5 was replaced with paper sludge (10 g/L) to evaluate its applicability for sustainable cellulase production. Cellulase production was evaluated at pH 9 and temperature 40 °C, in both paper sludge and normal M5 media. As shown in Fig. 3D, the cellulase production revealed the same pattern in both media with a slight increase in the cellulase titer in the M5 medium. Cellulase production was initiated on the first incubation day in M5 and paper sludge media (0.53 ± 0.02 and 0.13 ± 0.04 U/mL, respectively) and gradually increased to a maximum after 5 days of incubation to about 3.27 ± 0.15 and 2.95 ± 0.25 U/mL, respectively. The prolonged incubation time (after 5 days) adversely affected the cellulase activity, which could be attributed to protease production. These results are in agreement with other reported studies (Kalsoom et al. 2019; Ningthoujam and Dhingra 2022; Srivastava et al. 2022). The *Streptomyces rochei* growth was significantly increased by time up to 6 days of incubation in the M5 medium up to a cell mass of 0.29 g/mL. After 6 days, the increase in cell growth was insignificant and finally decreased to 0.28 g/mL on the 8th day. On the other hand, the cellulose residues from paper sludge hydrolysis greatly interfere with the cell mass determination in the paper sludge medium. The incubation period for cellulase production differs according to the type strain *Trichoderma reesei* (4 days)

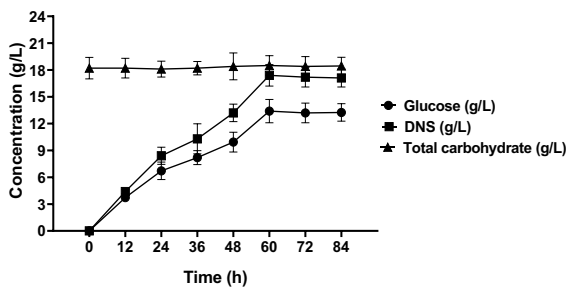


Fig. 4 The paper sludge hydrolysis process through the cellulase enzyme from *Streptomyces rochei* isolate represents the total carbohydrate contents, reducing sugars, and released glucose concentrations (g/L)

(Darabzadeh et al. 2019), *Enhydrobacter* sp. ACCA2, *Penicillium oxalicum* and *Bacillus subtilis* (3 days) (Malik et al. 2022; Premalatha et al. 2015; Saini et al. 2015) and *Mucor circinelloides* and *Mucor hiemalis* (5 days) (Al Mousa et al. 2022). Collectively the results asserted the good potential of paper sludge for economic and sustainable cellulase production.

Enzymatic hydrolysis of paper sludge using cellulase from *Streptomyces rochei*

Paper sludge high availability as a main waste from the paper manufacturing process represents a dual challenge for the environment and paper industry sectors (Duncan et al. 2020). The fermentation medium represents 30% of BC production costs; hence, the application of paper sludge for BC production could reduce its environmental impact and reduce the implemented cost (Duncan et al. 2020). The results of the enzymatic hydrolysis of paper sludge are illustrated in Fig. 4. We can observe that the total carbohydrate results indicated a high sugar content of the paper sludge of about 18 g/L, which is mostly in cellulose and hemicellulose form as indicated in the chemical analysis (Table S4). The initial simple sugar and glucose contents of crude paper sludge were very low or absent, as indicated in Fig. 4. The inability of *L. plantarum* to hydrolyze complex cellulosic materials was widely reported and accepted; hence, pre-hydrolysis for complex cellulosic sources is a prerequisite for supporting BC production (El-Gendi et al. 2023b). Initially, the paper sludge was mechanically homogenized in the hydrolysis buffer to increase enzyme accessibility to cellulosic fibers (Akintunde

et al. 2022; Mais et al. 2002). The enzymatic hydrolysis of paper sludge significantly increased the simple sugar contents to a maximum after 60 h, as indicated in the glucose and reducing sugars (about 13.4 and 17.4 g/L, respectively). Increasing the hydrolysis time after 60 h insignificantly affected the release of the simple sugars, which could be attributed to enzyme inactivation (feedback inactivation) with released glucose units (da Rosa-Garzon et al. 2022). The results asserted the efficiency of the applied hydrolysis process, as indicated by the insignificant difference between the maximum released reducing sugar and total carbohydrate contents (about 1.1 g), which is in line with other studies (Duncan et al. 2020; El-Gendi et al. 2023b).

BC production from paper sludge through batch and fed-batch fermentation

Paper sludge was obtained from the Quena Paper Industry Company (Kous-Quena, Egypt). This company used about 250 tons/day of sugarcane bagasse for the paper industry, and about 3–5 tons/day of paper sludge as waste reject during paper manufacturing process as illustrated in Figure S4. The obtained paper sludge without any pretreatment was chemically characterized according to TAPPI standards (moisture: TAPPI T208 om-84 (TAPPI 1984), ash: TAPPI T211om-93 (TAPPI 1993) lignin: TAPPI T222 om-83 (TAPPI 1983), hemicellulose: TAPPI T257 om-85 (TAPPI 1985) and α -cellulose: TAPPI T203 om-83 (TAPPI 1983), as summarized in Table S3. We can observe that the high content of ash is due to the presence of calcium carbonate as filler during the papermaking process, while the low content of lignin is due to the multiple bleaching processes that include three steps of chlorine oxide followed by oxygen and then chlorine oxide (according to the company conditions). On the other hand, the cellulose content in paper sludge represents common and high percentage of the constituent. Subsequently, it is very important for releasing sugar contents during the enzymatic hydrolysis action (Saleh et al. 2022a). During the papermaking process, several amounts of sludge were obtained as residual material due to its fine fiber structure. This fiber, or paper sludge, was used as a sustainable and cheap carbon source for the evaluation of BC production using batch and fed-batch fermentation. The fermentation

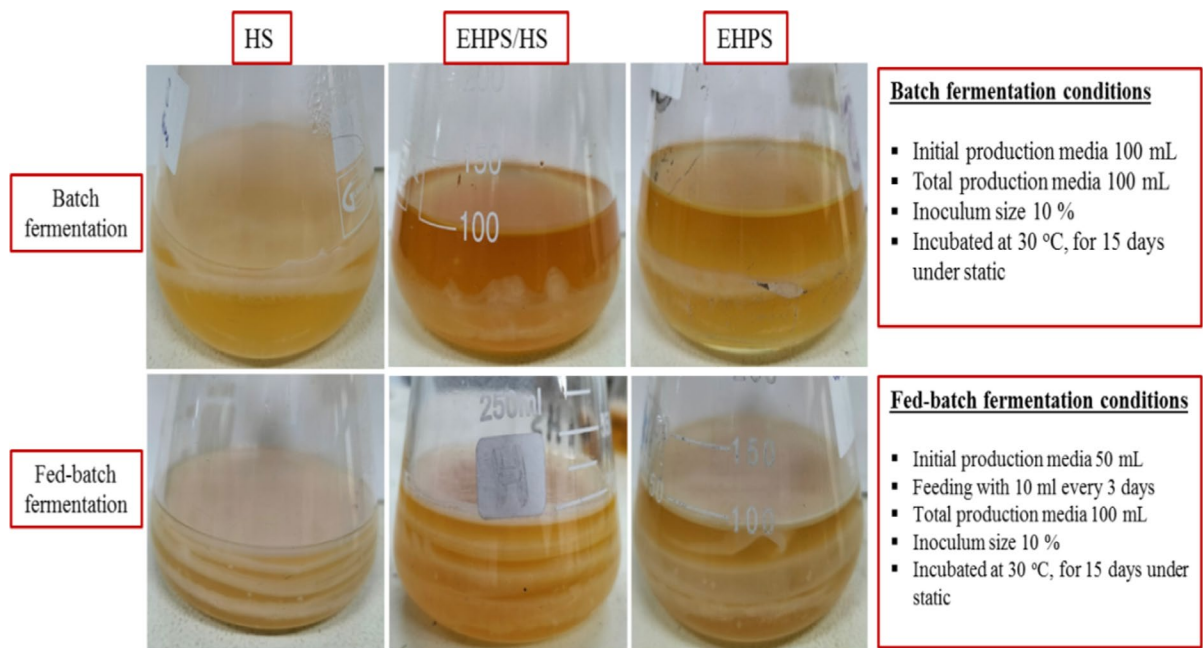


Fig. 5 The effect of batch and fed-batch fermentation strategies on BC yield using three BC production media HS, EHPS/HS (enzymatically hydrolyzed paper sludge supplemented with glucose-free HS medium), and EHPS (enzymatically hydrolyzed paper sludge)

strategies for BC production play an important role in enhancing BC production. The batch fermentation depends on the use of full media volume at the beginning of fermentation time (no further media was added), as reported in several studies (Lin et al. 2022; Tapias et al. 2022; Wang et al. 2021b). On the other hand, fed-batch fermentation refers to addition of fresh media during fermentation (at specific time points) as reported by (Aytekin et al. 2016; Cakar et al. 2014; Shezad et al. 2010). To determine the effect of batch and fed-batch fermentation on BC production, three different media recipes (HS, EHPS/HS, and EHPS) were evaluated (Fig. 5). According to our results obtained during batch fermentation, the HS medium produced more BC than EHPS and then EHPS/HS, with BC production of 1.97, 1.06, and 0.67 g/L, respectively. These findings show that

adding glucose-free HS to EHPS had no significant effects, indicating that EHPS can be used as a sustainable source of BC production. On the contrary, during the fed-batch fermentation of BC production, the HS media report a higher yield with the same BC production observed for both EHPS/HS and EHPS media. When comparing two types of fermentations, the observed data in Table 1 clearly showed that the BC production based on the fed-batch fermentation increased about 2.1, 4.6, and 2.9-folds more than the batch fermentation when using HS, EHPS/HS, and EHPS media, respectively. Cavka et al., reported that the fiber sludge obtained from the sulfate and sulfite processes was enzymatically hydrolyzed and used for BC production to obtain 2 g/L from an undiluted hydrolysate of both sulfate and sulfite paper sludge (Cavka et al. 2013), and this result is less than that

Table 1 BC production using batch and fed-batch fermentation strategies

BC parameters	Batch fermentation			Fed-batch fermentation		
	HS	EHPS/HS	EHPS	HS	EHPS/HS	EHPS
Production g/L	1.97 ± 0.24	0.67 ± 0.09	1.06 ± 0.38	4.13 ± 0.44	3.09 ± 0.08	3.10 ± 0.09
Yield %	9.85 ± 1.05	3.85 ± 0.08	6.09 ± 0.27	20.65 ± 2.53	17.75 ± 2.07	17.81 ± 0.15
Productivity %	12.6 ± 2.11	4.46 ± 0.55	7.06 ± 0.73	27.53 ± 2.19	20.60 ± 2.07	20.66 ± 2.24

obtained from the current study based on the fed-batch fermentation (3.10 g/L). Overall, the application of fed-batch strategy revealed significant BC production ability compared to batch fermentation, these findings agree with other reported studies (Kim and Han 2022; Sharma et al. 2021). The mechanism of BC production by batch and fed-batch fermentation was evaluated, as the BC was produced by batch static culture in the form of gel-like at the air–liquid interface. Once BC gel-like material formed, the production process was stopped due to the nutrients consumed with oxygen limitation. On the other hand, the fed-batch fermentation of BC production was confirmed by adding a fresh amount of media onto the BC gel-like at the air–liquid interface so that the newly formed BC could stack up successfully and become a single piece of BC with a desired thickness due to the newly added media which already activated bacteria take in enough nutrients and oxygen (Hsieh et al. 2016; Kim and Han 2022). Intermittent feeding in this way will continue BC synthesis and increase BC production. There is less information available in the literature that has studied the efficiency of different fermentation strategies for BC production, as presented in Table S5.

Microstructural characterization of BC samples

SEM micrographs of the BC surface prepared by batch and fed-batch fermentation are illustrated in Fig. 6. The BC membranes obtained from batch fermentation using the three different media displayed a nonporous three-dimensional network structure with randomly arranged fibrils and a variety of empty spaces. Interestingly, the different media compositions insignificantly affected the resulting BC structure, which is in agreement with another study (Kim and Han 2022). On the other hand, the BC membranes obtained by the fed-batch strategy revealed densely packed highly reticulated network structures with no obvious pores. During fed-batch fermentation of BC, a formation of new loosely-knitted intertwined nanofibers is visible over the surface of the underside fibers, which could be attributed to the formation of a young pellicle after dumping media directly above on existing pellicle. Overall the results indicated insignificant differences among the samples, which are in agreement with other studies (Dubey et al. 2018; Sharma et al. 2021). HS showed homogeneous and continuous sheets with compact morphology while EHPS/HS

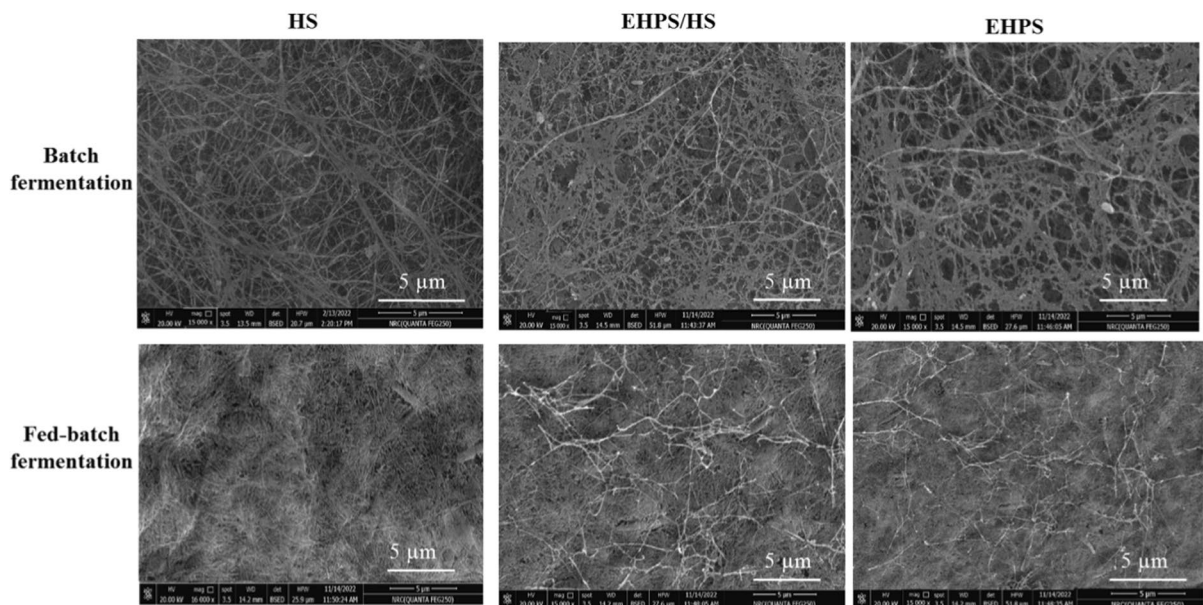


Fig. 6 The effect of batch and fed-batch fermentation strategies on BC structure as illustrated through SEM microscopy using three BC production media HS, EHPS/HS (enzymati-

cally hydrolyzed paper sludge supplemented with glucose-free HS medium), and EHPS (enzymatically hydrolyzed paper sludge)

and EHPS exhibited a random arrangement of ribbon-shaped microfibrils with different sizes and the surfaces are becoming more and more compact. The

average nanofiber diameters of the BC membranes obtained from HS, EHPS/HS, and EHPS media were found to be 78.8, 113.1, and 144.5 nm during

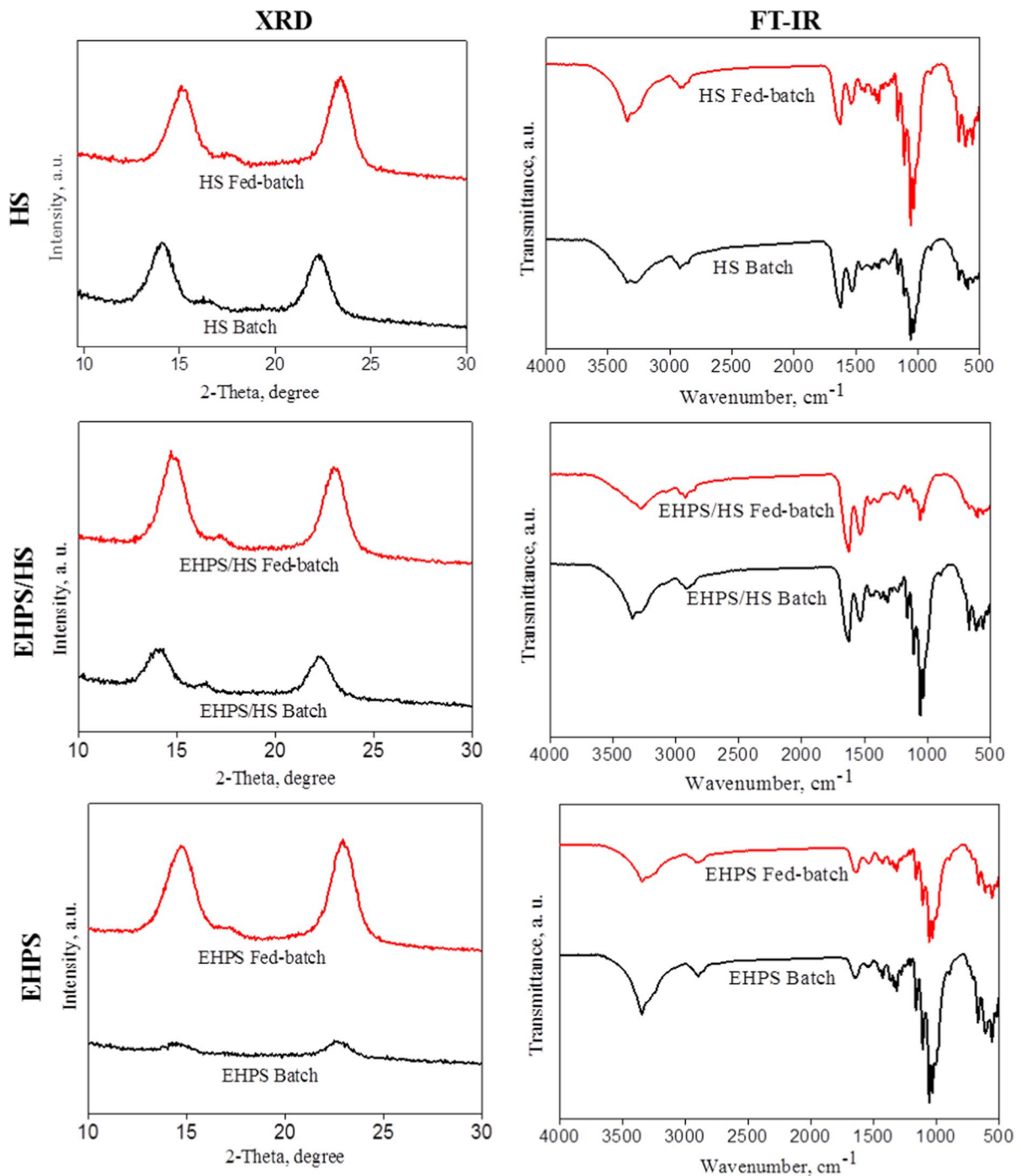


Fig. 7 XRD patterns and FT-IR spectra analysis of BC produced from HS, EHPS/HS and EHPS at batch (represented in black color) and fed-batch fermentation (represented in red lines)

batch fermentation and 54.4, 88.4, and 97.6 nm during fed-batch fermentation, respectively (Fig. S5). While the pore size diameters of the BC obtained from HS, EHPS/HS, and EHPS media (Fig. S6) were found to be 0.35, 0.71, and 0.92 μm during batch fermentation and 0.22, 0.35, and 0.49 μm during fed-batch fermentation, respectively as presented in Figure S6. The average nanofiber and pore size diameters of BC obtained from batch fermentation showed a thicker diameter than those obtained from fed-batch fermentation. Overall, we can observe that the fermentation methods and media composition of BC (batch and fed-batch fermentation) affect the morphology, fiber distribution, fiber diameter, and pore size (Kuo et al. 2019; Shezad et al. 2010).

On the other hand, Fig. 7 represents the XRD patterns of the BC membranes produced using the three different media in batch and fed-batch cultivation modes. BC shows three main characteristic diffraction peaks attributed to the crystallographic planes of (100), (010), and (110) at 2θ equal to 14.5, 16.6, and 22.7, respectively. The XRD results of the BC produced through batch and fed-batch fermentation are relatively different. In the case of fed-batch fermentation, the BC membranes have a different appearance and lower peak intensities as compared to batch fermentation. The reduction in peak intensity could be associated with the creation of amorphous BC. For BC produced by the fed-batch technique, the position of the (010) and (110) peaks were shifted to higher values of 2θ relative to BC produced by batch fermentation. We can observe that, the cultivation method has an effect on cellulose fractions, while the

media composition has no significant effects. These results are in agreement with another study (Shezad et al. 2010). The CI values of the BC obtained from HS media by batch and fed-batch fermentation recorded were 76 and 74%, respectively. However, CI values decreased for EHPS media in batch and fed-batch fermentation to reach about 70 and 44%, respectively. Also, for the BC obtained from EHPS/HS by batch and fed-batch fermentation, the CI values recorded were 71 and 58%, respectively. It has been reported that the addition of natural fibers such as waste hydrolysate to the BC production medium has a significant influence on the nanofibers and pore size diameter, which consequently may influence the crystallinity of the fibers. A possible explanation is that the incorporation of extracts may result in repulsion between nanofibers (El-Gendi et al. 2023b).

Otherwise, Fig. 7, displays the FT-IR spectra of BC prepared through batch and fed-batch fermentation with different media compositions. In the case of HS, the BC formed via batch strategy is completely like the BC formed through fed-batch fermentation. The formed BC showed the characteristic peaks reported for BC in previous studies (El-Gendi et al. 2023b; Saleh et al. 2022b). For EHPS/HS and EHPS, most of the characteristic vibrations in the spectra are the same as BC with small differences. For example, the BC produced by using EHPS/HS and EHPS through the fed-batch technique showed a weak peak at 3300 cm^{-1} , corresponding to the intramolecular hydrogen bond of the hydroxyl groups. This may refer to changing the intensity and the hydroxyl groups, which may reflect changes in the intermolecular hydrogen bonds and crystallinity. Overall, the

Table 2 Functional and chemical bonds of BC membranes from HS, EHPS/HS and EHPS media by batch and fed-batch fermentation as illustrated through FR-IR analysis

Assignment	Band position (cm^{-1})					
	Batch-fermentation			Fed-batch fermentation		
	HS	EHPS/HS	EHPS	HS	EHPS/HS	EHPS
OH	3383	3344	3346	3346	3274	3344
CH_2	2921	2916	2896	2925	2923	2894
Asymmetric C–H	1448	1436	1427	1427	1452	1427
Symmetric C–H	1371	1371	1359	1373	1385	1369
C–O–C	1161	1160	1162	1162	1161	1161
C–OH	1110	1108	1108	1108	1108	1108
C–C–OH	1056	1056	1058	1058	1056	1056
C–H	894	894	898	896	-	896

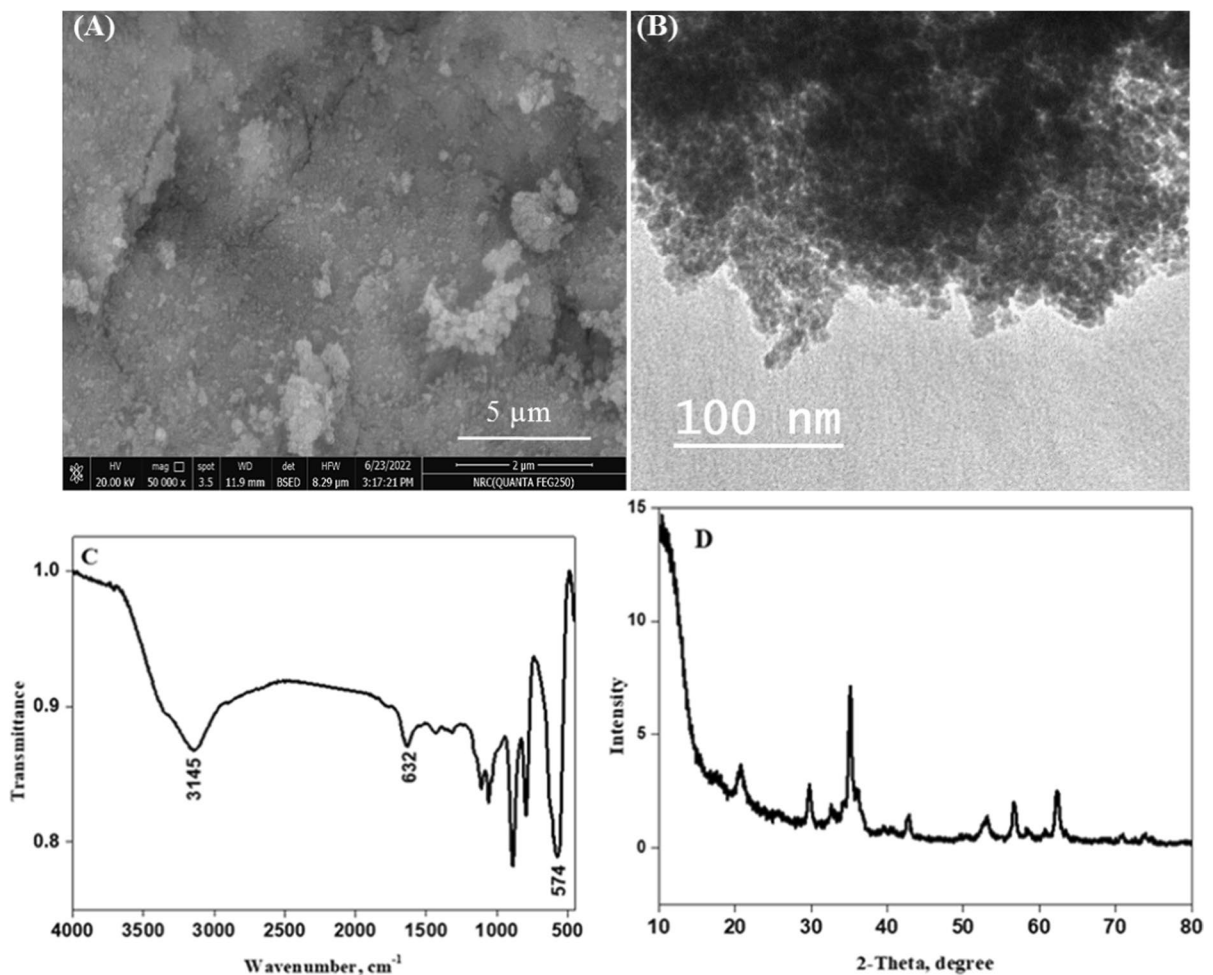


Fig. 8 Instrumental characterization of the prepared BC/Fe₃O₄ nanocomposite reveals the composite morphology through SEM (A), and TEM microscopy (B), the nanocomposite func-

tional groups through FT-IR spectra (C), and crystallinity through XRD analysis (D)

bands' position in the FT-IR spectra for all samples at different media compositions and cultivation methods (Table 2) were in the same range and did not show any significant difference (Shezad et al. 2010).

Characterization of BC/Fe₃O₄ nanocomposite

The morphology of BC/Fe₃O₄ nanocomposite was studied using SEM analysis as displayed in Fig. 8A. The SEM image of the in situ preparation of BC with Fe₃O₄ nanoparticles showed the formation of regular particles with a diameter of less than 50 nm. Moreover, the formed nanoparticles appear to have uniform morphology, likely due to the BC/Fe₃O₄

nanocomposite interaction which reduces the attractive forces between nanoparticles and decreases their aggregation tendency (Salama et al. 2018). TEM analysis was developed to demonstrate the internal shape of BC/Fe₃O₄ nanocomposite. Figure 8B exhibited a spherical-shaped appearance of the BC/Fe₃O₄ nanocomposite. The particle size ranges from 5 to 10 nm. The characteristic FT-IR functional groups for BC/Fe₃O₄ nanocomposite are observed in Fig. 8C. Prominent peaks were produced by the Fe–O stretch at around 574 cm⁻¹. Furthermore, Fe₃O₄ formation is established by the peak at 1632 cm⁻¹, which is formed at higher Fe²⁺/Fe³⁺ ratios, according to the literature (Nidheesh et al. 2014). A prominent peak for

the O–H is assigned to 3145 cm^{-1} , characteristic of the presence of BC. It is possible that the OH peak is due to hydroxyl functional groups in iron or to water absorbed into iron (Muzenda and Arotiba 2022). The BC/Fe₃O₄ nanocomposite diffraction pattern produces a pattern with broad reflections indicative of small crystallites and poor crystallographic correlation developing from the existence of BC (Fig. 8D). The presence of the characteristic peaks at $2\theta = 29.5^\circ$, 34.9° , 43.1° , 56.5° , and 62° in the XRD pattern of the nanocomposite may indicate the cubic spinel structure of the Fe₃O₄ (Salama et al. 2018).

Optimization of MO decolorization through BBD

To find the optimal level of each selected parameter, a second multifactorial BBD (RSM) was used to achieve the maximum MO decolorization. Based on the literatures, three factors were evaluated in the MO decolorization process: medium pH (X1), BC/Fe₃O₄ nanocomposite concentration (X2), and removal time (X3) at three varying levels (−1, 0, and +1), as shown in Table S2. The results in Table 3 revealed a significant variation in the degree of MO decolorization related to different trials (different conditions) from 19.50% to 82.69% (about 63.19% variation), which indicated the direct impact of the optimization process upon MO decolorization. As RSM design, a

second-order polynomial equation was fitted to the experimental results of MO decolorization to evaluate the optimal point within experimental constraints (Eq. 5). According to the regression analysis result, Eq. 4 could be re-written as follows:

$$Y_{\text{MO decolorization}} = 24.4 - 22.4(X1) + 7.9(X2) + 1.5(X3) + 8.8(X1X2) - 3.93(X1X3) + 1.1(X2X3) + 28.23(X1)^2 + 5.6(X2)^2 - 1.18(X3)^2$$

where Y is MO decolorization (%) and X1, X2, and X3 are pH, BC/Fe₃O₄ nanocomposite concentration, and removal time, respectively. At the model level, the better correlation measures for evaluating the regression equation are the multiple correlation coefficients R and the determination coefficient R² (adj-R²). Statistically, the closer the two values (R² and adj-R²) to 1, the more and better correlation between the measured and predicted values at the model level. The ANOVA analysis (Table S5) indicated that R² and adj-R² values for MO decolorization were 0.99 and 0.96, respectively, which indicated the high accuracy of the applied model.

The optimal levels of the three components as obtained from the maximum point of the polynomial model were estimated using the solver function of Microsoft Excel tools, and the relative

Table 3 BBD for the studied factors (X1–X3): pH, BC/Fe₃O₄ nanocomposite conc. (mg/25 mL), and interaction time (min) representing their coded (−1, 0, and 1) and real values (between brackets) with measured and predicted percentages of MO decolorization (design response)

Trial	Parameters			MO decolorization %	
	pH (X1)	BC/Fe ₃ O ₄ nanocomposite conc. (X2)	Time (X3)	Measured response	Predicted response
1	−1 (3)	−1 (0.1)	0 (40)	80	81.88375
2	1 (9)	−1 (0.1)	0 (40)	24.04	19.36625
3	−1 (3)	1 (0.3)	0 (40)	74.72	79.39375
4	1 (9)	1 (0.3)	0 (40)	54.11	52.22625
5	−1 (3)	0 (0.2)	−1 (20)	71.65	68.475
6	1 (9)	0 (0.2)	−1 (20)	28.11	31.4925
7	−1 (3)	0 (0.2)	1 (60)	82.69	79.3075
8	1 (9)	0 (0.2)	1 (60)	23.43	26.605
9	0 (6)	−1 (0.1)	−1 (20)	19.50	20.79125
10	0 (6)	1 (0.3)	−1 (20)	35.33	33.83125
11	0 (6)	−1 (0.1)	1 (60)	20.12	21.61875
12	0 (6)	1 (0.3)	1 (60)	40.24	38.94875
13	0 (6)	0 (0.2)	0 (40)	24.17	24.41333
14	0 (6)	0 (0.2)	0 (40)	23.80	24.41333
15	0 (6)	0 (0.2)	0 (40)	25.27	24.41333

values -1 , -1 , and 1 represent the optimal points for pH, BC/Fe₃O₄ nanocomposite concentration, and removal time, respectively (Figure S7). Consequently, the composition and parameters of the optimized medium were as follows: media pH 3.0, BC/Fe₃O₄ nanocomposite concentration 0.1 (mg/dL), removal time 60 min with a predicted MO decolorization of 85.04%. One of the most important parameters that influence MO decolorization is the decolorization pH, which can significantly alter the ionization of dye molecules as well as the surface charge of the adsorbent (Bhowmik et al. 2020). From the obtained results, we can observe that the medium pH inversely affected the MO decolorization. At lower pH values (below pH 5.0), the MO decolorization rate was greatly enhanced, whereas, at high pH values (above pH 5.0), the MO decolorization was significantly inhibited, which could be attributed to Fe⁺³ precipitation at high pH values (Adachi et al. 2022; Bhowmik et al. 2020) (Jawad et al. 2022). The maximum MO decolorization was achieved at pH 3, which is consistent with Adachi and his colleagues' reported maximum MO decolorization of about 94.9% at pH 3 (Adachi et al. 2022). Other studies by Hasanpour et al., and Zhang et al., report MO decolorization by 98% and $\geq 93\%$, respectively at the same pH value (Hasanpour et al. 2021) (Zhang et al. 2020). The optimum amount of adsorbent (BC/Fe₃O₄) for maximum MO decolorization was evaluated at three BC/Fe₃O₄ nanocomposite concentrations. The results revealed higher efficiency for MO decolorization at low concentrations of adsorbent (0.1 mg/dL). Increasing the BC/Fe₃O₄ nanocomposite concentration over 0.1 mg/dL, insignificantly affected the MO decolorization, which could be attributed to sufficient and large numbers of adsorption sites (Haldorai et al. 2015; Tanhaei et al. 2015). Contacting time is another important parameter in the dye adsorption process. The results indicated a direct relationship between time and MO decolorization, as increasing the time significantly increased the MO decolorization with a maximum of about 85.04% of MO decolorization after 60 min, which is in line with (Attallah et al. 2016).

Several studies reported the optimization of MO decolorization through OVAT and statistical methods as indicated in Table 4. The statistical methods are privileged by their ability to elucidate the studied variables'

interactions and their impact on the measured responses (El-Gendi et al. 2023a). In this experiment, the effects of studied variable interactions were visualized by 3D surface plotting, representing any two independent parameters while maintaining the third parameter at its middle levels (Fig. 9). These graphs indicated that lower levels of pH promoted high MO decolorization levels, while increasing the medium pH adversely affected the BC/Fe₃O₄ nanocomposite concentration and increased the dye removal time. In contrast, higher MO decolorization levels were achieved by increasing the BC/Fe₃O₄ nanocomposite concentration above 0.2 mg/dL, especially when the removal time was around 40 min. Any further increase in the BC/Fe₃O₄ nanocomposite concentration or removal time didn't significantly affect the MO decolorization.

In the last step of the optimization process, a verification experiment was performed to determine the accuracy of the quadratic polynomial under the predicted optimal conditions from the BBD model. Under optimum conditions, the estimated MO decolorization in the laboratory was 83.5%, whereas the predicted value from the polynomial model was 85.04%. Thereby, these results revealed a high agreement between the predicted and the experimental results of 98.2%, which is clear evidence of model validation. Models with $\leq 5\%$ differences between measured and predicted results are considered statistically reliable and acceptable (Bajpai and Katoch 2021). According to the results, the final conditions for MO decolorization were medium pH 3, and BC/Fe₃O₄ nanocomposite concentration of 0.1 mg/dL after 60 min incubation under shaking conditions (200 rpm) at room temperature. The constancy between predicted and measured responses in models applied for optimizing MO decolorization was varied, whereas 100% accuracy was reported by a bacterial consortium (Ghanem et al. 2012), 93.5% accuracy was also reported through *Acacia mangium* wood/activated carbon (Danish and Hashim 2014).

Adsorption kinetics study

The contact time for dye removal is of great importance for nanocomposites to be used effectively in wastewater treatment. Hence, the removals of MO at different initial concentrations (50 and 150 ppm) were measured at different times, as illustrated in Fig. 10. It is clear that the adsorption capacities increased with adsorption time. However, the adsorption equilibrium time does

Table 4 Comparison of MO adsorption capacity with previously reported adsorbents

Adsorbent	Optimization design	Optimized conditions	MO decolorization %	Reference
BC/Fe ₃ O ₄	RSM-BBD	Dose (0.1 mg/dL), time (60 min), and pH (3)	85	Current study
Chitosan/Al ₂ O ₃ /Fe ₃ O ₄	OVAT	Dose (0.4 g/L), time (90 min), and pH (4)	93	Tanhaei et al. (2015)
Polyaniline nano-adsorbent	RSM-CCD	Dose (0.8 g/L), time (30.5 min), temperature (45°C), and pH (6)	86.3	Karri et al. (2018)
Lignin/mordenite/zeolites	RSM-BBD	Dose (0.27 g/L, time (30 min), and pH (7)	40	Saini et al. (2021)
Polypyrrole/magnetic/chitosan	OVAT	Dose (100 mg), time (40 min), and pH (4.5)	80	Alsaiari et al. (2021)
Mix of CaFe ₂ O ₄ /MnFe ₂ O ₄	RSM-CCD	Dose (0.58 g/L), time (24 min), and dye concentration (98.37 mg/L)	99.8	Bhowmik et al. (2020)
Graphene/Fe ₃ O ₄	ND	ND	99.24	Arshad et al. (2018)
Electro-fenton Process	OVAT	Current intensity (80 mA), Fe ²⁺ (0.232 mM), pH (3), temperature (30°C) and dye concentration (60 mg/L)	94.9	Adachi et al. (2022)
Chitosan/tripolyphosphate/nanotitania	RSM-BBD	Dose (0.09 g/L), TiO ₂ (50%), pH (4) and temperature (40 °C)	87.27	Jawad (2020)
Cellulose/zinc oxide aerogel	RSM-CCD	Photocatalyst dosage (9 g/L), pH (3), MCC concentration (9 g) and dye concentration (10 ppm)	98	Hasanpour et al. (2021)
<i>Acacia mangium</i> wood/activated carbon	RSM-FCCD	Dose (0.515 g/L), time (24 h) and temperature (55°C)	90.5	Danish and Hashim (2014)
Chitosan/ Fe ₃ O ₄ nanoparticles	OVAT	Dose (0.5 g/L), time (5 min) and pH (8)	97	Haldorai et al. (2015)
Fe ₃ O ₄ /pectin	ND	pH (2)	12.5	Attallah et al. (2016)
Bacterial consortium	RSM-DOEs	Mixed of three bacterial culture, and time (48 h)	≥ 84	Ayed et al. (2010)
Chitosan/tannin/montmorillonite	OVAT	Dye concentration (60 mg/L), pH (7), and temperature (25°C)	95.62	Tahari et al. (2022)
Vanadium/titanium/ Fe ₃ O ₄	OVAT	Dose (4 g/L), pH (3), temperature (65°C), dye concentration (30 mg/L), and time (120 min)	97.82	Zhang et al. (2020)

ND= Not Detected

not change significantly by changing the initial concentration of dyes. At MO concentrations of 50 and 150 ppm, the MO adsorptions reached equilibrium after 2 h. In order to understand the mechanism of the adsorption process, two kinetic models, the pseudo-first-order and pseudo-second-order, were fitted to evaluate the adsorption data, and the corresponding equations were represented as follows:

$$\log(q_e - q_t) = \log(q_e) - \frac{K_1}{2.303}t \quad (8)$$

$$\frac{t}{q_t} = \frac{t}{q_e} + \frac{1}{K_2 q_e^2} \quad (9)$$

where q_t (mg/g) is the adsorption capacity at time t , q_e (mg/g) is the equilibrium adsorption capacity, K_1 (h⁻¹) is the pseudo-first-order rate constant, and K_2 (mg/g h⁻¹) is the pseudo-second-order rate constant.

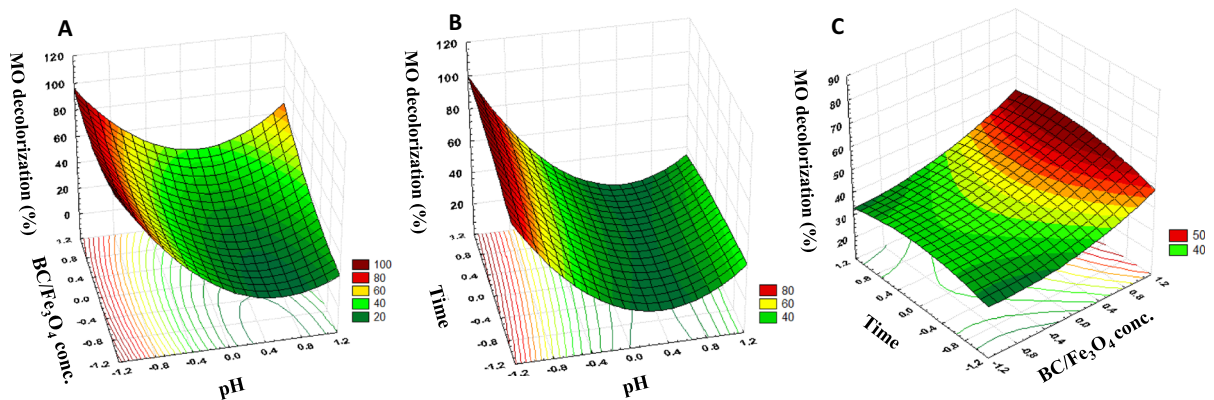


Fig. 9 The 3D surface plots revealing the effect of variable interactions on X-axes including medium pH with BC/Fe₃O₄ nanocomposite conc. (A), medium pH with interaction time

(B), and BC/Fe₃O₄ nanocomposite conc. and interaction time (C) upon final MO decolorization rate (on Y-axes)

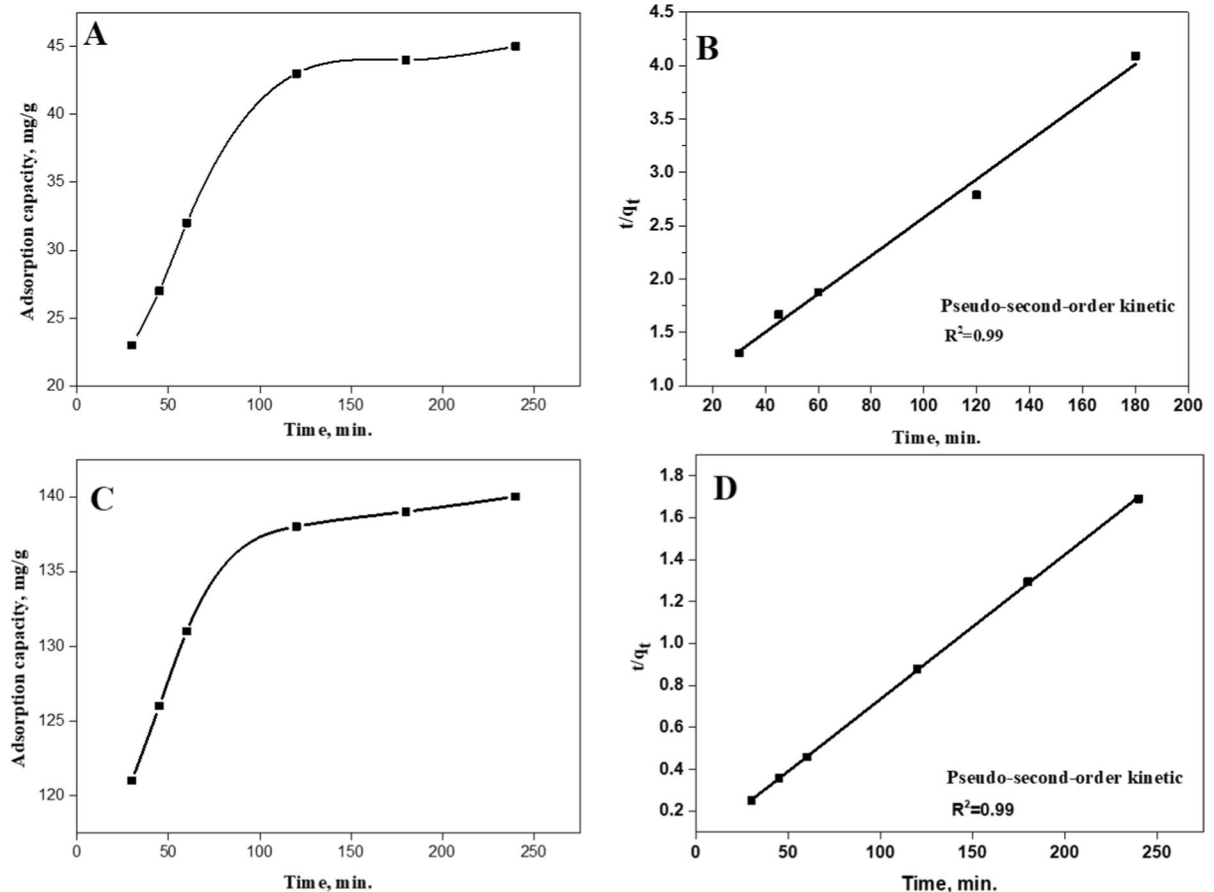


Fig. 10 Effect of the adsorption time on adsorption capacity (MO concentration: 100 mg/L; adsorbent: 0.05 g/50 mL at pH 7) at 50 and 150 ppm (A and C, respectively) and plots of the pseudo-second-order models (B and D)

Table 5 Kinetic parameters for MO adsorption by BC/Fe₃O₄ nanocomposite at different MO concentrations

MO concentration	$q_{e, \text{exp}}$ (mg/g)	Pseudo first order-model			Pseudo second-order model		
		$q_{e, \text{cal}}$ (mg/g)	K_1 (min ⁻¹)	R^2	$q_{e, \text{cal}}$ (mg/g)	K_2 (g/mg/min)	R^2
50 ppm	45	37	0.018	0.93	55	4.2×10^{-4}	0.99
150 ppm	140	31	0.016	0.97	147	10.2×10^{-4}	0.99

The fitted curves at different concentrations are demonstrated in Fig. 10, and regression coefficients (R^2), rate constants, and other parameters calculated by the two models are listed in Table 5. According to R^2 , the adsorption kinetics of MO was more approximately described by the pseudo-second-order model, where the R^2 was 0.99, and the maximum adsorptions matched well with the experimental data.

Effect of MB concentration and equilibrium isotherm

The experimental adsorption isotherm of BC/Fe₃O₄ nanocomposite was plotted by determining the q_e with different aqueous MO concentrations. As shown in Figure S8, the q_e of the adsorbent for MO increased with increasing their initial concentrations, which may be attributed to the improvement of the mass transfer driving force. Further, the experimental adsorption isotherm data were fitted by Langmuir Eq. 10 and Freundlich Eq. 11 models.

$$\frac{C_e}{q_e} = \frac{K_s}{q_{\text{max}}} + \frac{C_e}{q_{\text{max}}} \quad (10)$$

$$\log q_e = \frac{1}{n} \log C_e + \log p \quad (11)$$

With batches containing different MO concentrations (50–900 mg/L), the removal of MO dye was enhanced by increasing the initial concentration. BC/Fe₃O₄ nanocomposite exhibited higher adsorption capacity, which indicates the significance of the developed Fe₃O₄ nanoparticles in creating attraction sites with the MO. Freundlich models discuss multilayer adsorption, while Langmuir models assume uniform adsorption at definite localized sites. Figure S8, illustrates the adsorption isotherms of MO on BC/Fe₃O₄, and Table S4 lists the corresponding data. Based on the regression coefficient (R^2) values calculated by adsorption isotherms, Langmuir's isotherm was found to be a good fit for the experimental data ($R^2=0.96$) indicating homogeneous adsorption sites

on the BC/Fe₃O₄ nanocomposite surface. The Langmuir isotherms determined the maximum adsorption capacity (q_{max}) for MO on BC/Fe₃O₄ nanocomposite to be 714 mg/g. The linear coefficient of the Freundlich model, which is based on adsorption on heterogeneous surfaces, was 0.66. According to these results, the Freundlich model did not effectively explain the adsorption processes of the BC/Fe₃O₄ nanocomposite for MO decolorization. The values of the Freundlich-model-constant: P (38) and n (1.75) for BC/Fe₃O₄ nanocomposite were shown in Table S6.

Conclusion

The current study highlights the economic production of both cellulase and BC based on environmentally hazardous waste as paper sludge. The cellulase-producing strain was locally isolated and identified on biochemical and molecular bases as *Streptomyces rochei* with an identity percentage of 99%. The identified strain revealed significant potential for cellulase production using paper sludge, nearly equal to that on CMC-medium. The results asserted the applicability of paper sludge for economic and sustainable cellulase production through *Streptomyces rochei* local isolate. The produced cellulase was successfully applied for paper sludge hydrolysis, whereas the resulting hydrolysate was applied for BC production. Different media recipes, based on the enzymatically hydrolyzed paper sludge, in addition to two fermentation strategies, were evaluated for maximum BC production. The results indicated variation in the BC production yield that was largely related to fermentation strategy rather than medium compositions. Fed-batch fermentation revealed a maximum BC production of about 3.10 g/L. The instrumental analysis approved the applicability of paper sludge for pure BC production with no obvious changes in the cellulose structure or functional groups. However, the BC membranes resulting from fed-batch fermentation revealed a thicker fiber diameter and higher crystallinity indexes, which could be the basis for targeted

fiber diameter studies. Furthermore, the BC/Fe₃O₄ nanocomposite showed an exponential potential for MO decolorization up to 83.5% even at very low BC/Fe₃O₄ nanocomposite concentrations. The medium pH represents the main controlling factor for MO decolorization through BC/Fe₃O₄ nanocomposite as indicated in the statistical results. Therefore, the current study represents an eco-friendly and cost-effective approach for sustainable cellulase and BC production based on paper sludge and implications propose the BC/Fe₃O₄ nanocomposite as promising adsorbent for the rapid removal of dye from contaminated water.

Author contribution A.K.S.: Conceptualization, formal analysis, investigation, methodology, writing—review & editing data curation. A.S.: Formal analysis, investigation, methodology & writing original draft. A.S.B.: Methodology. M.A.D.: Methodology. H.E–G.: Conceptualization, formal analysis, investigation, methodology, writing—review & editing data curation.

Funding Open access funding provided by The Science, Technology & Innovation Funding Authority (STDF) in cooperation with The Egyptian Knowledge Bank (EKB).

Data availability The datasets used and/or analyzed during the current study are available from the corresponding author on reasonable request.

Declarations

Competing interests The authors declare no competing interests.

Open Access This article is licensed under a Creative Commons Attribution 4.0 International License, which permits use, sharing, adaptation, distribution and reproduction in any medium or format, as long as you give appropriate credit to the original author(s) and the source, provide a link to the Creative Commons licence, and indicate if changes were made. The images or other third party material in this article are included in the article's Creative Commons licence, unless indicated otherwise in a credit line to the material. If material is not included in the article's Creative Commons licence and your intended use is not permitted by statutory regulation or exceeds the permitted use, you will need to obtain permission directly from the copyright holder. To view a copy of this licence, visit <http://creativecommons.org/licenses/by/4.0/>.

References

- Adachi A, Ouadrhiri FE, Kara M, El Manssouri I, Assouguem A, Almutairi MH, Bayram R, Mohamed HR, Peluso I, Eloutassi N (2022) Decolorization and degradation of methyl orange azo dye in aqueous solution by the electro Fenton process: Application of optimization. *Catalysts* 12:665
- Ahamed A, Vermette P (2009) Effect of culture medium composition on *Trichoderma reesei*'s morphology and cellulase production. *Bioresour Technol* 100:5979–5987
- Akintunde MO, Adebayo-Tayo BC, Ishola MM, Zamani A, Horváth IS (2022) Bacterial cellulose production from agricultural residues by two *Komagataeibacter* sp. *Strains Bioeng* 13:10010–10025
- Al Mousa AA, Hassane A, Gomaa AE-RF, Aljuriss JA, Dahmash ND, Abo-Dahab NF (2022) Response-surface statistical optimization of submerged fermentation for pectinase and cellulase production by *Mucor circinelloides* and *M. hiemalis*. *Fermentation* 8:205
- Alsaari NS, Amari A, Katubi KM, Alzahrani FM, Rebah FB, Tahoon MA (2021) Innovative magnetite based polymeric nanocomposite for simultaneous removal of methyl orange and hexavalent chromium from water. *Processes* 9:576
- Arshad A, Iqbal J, Ahmad I, Israr M (2018) Graphene/Fe₃O₄ nanocomposite: Interplay between photo-Fenton type reaction, and carbon purity for the removal of methyl orange. *Ceram Int* 44:2643–2648
- Attallah OA, Al-Ghobashy MA, Nebsen M, Salem MY (2016) Removal of cationic and anionic dyes from aqueous solution with magnetite/pectin and magnetite/silica/pectin hybrid nanocomposites: kinetic, isotherm and mechanism analysis. *RSC Adv* 6:11461–11480
- Ayed L, Khelifi E, Jannet HB, Miladi H, Cheref A, Achour S, Bakhrouf A (2010) Response surface methodology for decolorization of azo dye methyl orange by bacterial consortium: Produced enzymes and metabolites characterization. *Chem Eng J* 165:200–208
- Aytekin AÖ, Demirbağ DD, Bayrakdar T (2016) The statistical optimization of bacterial cellulose production via semi-continuous operation mode. *J Ind Eng Chem* 37:243–250
- Bajpai M, Katoch SS (2021) Reduction of COD from real gray-water by electro-coagulation using Fe electrode: Optimization through box-behnken design. *Mater Today: Proc* 43:303–307
- Baziramakenga R, Simard R (2001) Effect of deinking paper sludge compost on nutrient uptake and yields of snap bean and potatoes grown in rotation. *Compost Sci Util* 9:115–126
- Bhowmik M, Debnath A, Saha B (2020) Fabrication of mixed phase CaFe₂O₄ and MnFe₂O₄ magnetic nanocomposite for enhanced and rapid adsorption of methyl orange dye: statistical modeling by neural network and response surface methodology. *J Dispers Sci Technol* 41:1937–1948
- Box GE, Behnken DW (1960) Some new three level designs for the study of quantitative variables. *Technometrics* 2:455–475
- Cakar F, Özer I, Aytekin AÖ, Şahin F (2014) Improvement production of bacterial cellulose by semi-continuous process in molasses medium. *Carbohydr Polym* 106:7–13
- Cavka A, Guo X, Tang S-J, Winstrand S, Jönsson LJ, Hong F (2013) Production of bacterial cellulose and enzyme from waste fiber sludge. *Biotechnol Biofuels* 6:1–10
- Chukwuma OB, Rafatullah M, Tajarudin HA, Ismail N (2021) A review on bacterial contribution to lignocellulose

- breakdown into useful bio-products. *Int J Environ Res Public Health* 18:6001
- Cusidó J, Cremades L, Soriano C, Devant M (2015) Incorporation of paper sludge in clay brick formulation: ten years of industrial experience. *Appl Clay Sci* 108:191–198
- da Rosa-Garzon NG, Laure HJ, Rosa JC, Cabral H (2022) Valorization of agricultural residues using *Myceliophthora thermophila* as a platform for production of lignocellulolytic enzymes for cellulose saccharification. *Biomass Bioenergy* 161:106452
- Danish M, Hashim R (2014) MN mohamad ibrahim & othman sulaiman. *Wood Sci Technol* 48:1069–1083
- Danso B, Ali SS, Xie R, Sun J (2022) Valorisation of wheat straw and bioethanol production by a novel xylanase-and cellulase-producing streptomyces strain isolated from the wood-feeding termite. *Microcerotermes Species Fuel* 310:122333
- Daquioag JEL, Penuliar GM (2021) Isolation of actinomycetes with cellulolytic and antimicrobial activities from soils collected from an urban green space in the Philippines. *Int J Microbiol* 2021:1–14
- Darabzadeh N, Hamidi-Esfahani Z, Hejazi P (2019) Optimization of cellulase production under solid-state fermentation by a new mutant strain of *Trichoderma reesei*. *Food Sci Nutr* 7:572–578
- Dhar P, Pratto B, Cruz AJG, Bankar S (2019) Valorization of sugarcane straw to produce highly conductive bacterial cellulose/graphene nanocomposite films through in situ fermentation: kinetic analysis and property evaluation. *J Clean Prod* 238:117859
- Dubey S, Singh J, Singh RP (2018) Biotransformation of sweet lime pulp waste into high-quality nanocellulose with an excellent productivity using *Komagataeibacter europaeus* SGP37 under static intermittent fed-batch cultivation. *Bioresour Technol* 247:73–80
- Duncan SM, Alkasrawi M, Gurram R, Almomani F, Wiberley-Bradford AE, Singas E (2020) Paper mill sludge as a source of sugars for use in the production of bioethanol and isoprene. *Energies* 13:4662
- El-Gendi H, Taha TH, Ray JB, Saleh AK (2022) Recent advances in bacterial cellulose: a low-cost effective production media, optimization strategies and applications. *Cellulose* 56:1–39
- El-Gendi H, Abu-Serie MM, Kamoun EA, Saleh AK, El-Fakharany EM (2023) Statistical optimization and characterization of fucose-rich polysaccharides extracted from pumpkin (*Cucurbita maxima*) along with antioxidant and antiviral activities. *Int. J. Biol. Macromol.* 26:123372
- El-Gendi H, Salama A, El-Fakharany EM, Saleh AK (2023b) Optimization of bacterial cellulose production from prickly pear peels and its ex situ impregnation with fruit byproducts for antimicrobial and strawberry packaging applications. *Carbohydr Polym* 302:120383
- Fatima A, Yasir S, Ul-Islam M, Kamal T, Ahmad M, Abbas Y, Manan S, Ullah MW, Yang G (2022) Ex situ development and characterization of green antibacterial bacterial cellulose-based composites for potential biomedical applications. *Adv Compos Hybrid Mater* 5:307–321
- Fatokun EN, Nwodo UU, Okoh AI (2016) Classical optimization of cellulase and xylanase production by a marine Streptomyces species. *Appl Sci* 6:286
- García R, de la Villa RV, Vegas I, Frías M, de Rojas MS (2008) The pozzolanic properties of paper sludge waste. *Constr Build Mater* 22:1484–1490
- Ghanem KM, Al-Fassi FA, Biag AK (2012) Optimization of methyl orange decolorization by mono and mixed bacterial culture techniques using statistical designs. *Afr J Microbiol Res* 6:2918–2928
- Haghighi H, Gullo M, La China S, Pfeifer F, Siesler HW, Licciardello F, Pulvirenti A (2021) Characterization of bio-nanocomposite films based on gelatin/polyvinyl alcohol blend reinforced with bacterial cellulose nanowhiskers for food packaging applications. *Food Hydrocoll* 113:106454
- Haldorai Y, Kharismadewi D, Tuma D, Shim J-J (2015) Properties of chitosan/magnetite nanoparticles composites for efficient dye adsorption and antibacterial agent. *Korean J Chem Eng* 32:1688–1693
- Hasanpour M, Motahari S, Jing D, Hatami M (2021) Statistical analysis and optimization of photodegradation efficiency of methyl orange from aqueous solution using cellulose/zinc oxide hybrid aerogel by response surface methodology (RSM). *Arab J Chem* 14:103401
- Hestrin S, Schramm M (1954) Synthesis of cellulose by *Acetobacter xylinum*. 2. Preparation of freeze-dried cells capable of polymerizing glucose to cellulose. *Biochem J* 58:345
- Hsieh J-T, Wang M-J, Lai J-T, Liu H-S (2016) A novel static cultivation of bacterial cellulose production by intermittent feeding strategy. *J Taiwan Inst Chem Eng* 63:46–51
- Ibrahim MM, El-Zawawy WK, Abdel-Fattah YR, Soliman NA, Agblevor FA (2011) Comparison of alkaline pulping with steam explosion for glucose production from rice straw. *Carbohydr Polym* 83:720–726
- Javed Z, Tripathi GD, Mishra M, Dashora K (2021) Actinomycetes—the microbial machinery for the organic-cycling, plant growth, and sustainable soil health. *Biocatal Agric Biotechnol* 31:101893
- Jawad A (2020) Statistical optimization for dye removal from aqueous solution by cross-linked chitosan composite. *Sci Lett* 14:1–14
- Jawad AH, Sahu UK, Jani NA, Allothman ZA, Wilson LD (2022) Magnetic crosslinked chitosan-tripolyphosphate/MgO/Fe₃O₄ nanocomposite for reactive blue 19 dye removal: optimization using desirability function approach. *Surf Interfaces* 28:101698
- Jensen PR, Dwight R, Fenical W (1991) Distribution of actinomycetes in near-shore tropical marine sediments. *Appl Environ Microbiol* 57:1102–1108
- Joshi S, Garg V, Kataria N, Kadirvelu K (2019) Applications of Fe₃O₄@ AC nanoparticles for dye removal from simulated wastewater. *Chemosphere* 236:124280
- Jung DU, Yoo HY, Kim SB, Lee JH, Park C, Kim SW (2015) Optimization of medium composition for enhanced cellulase production by mutant *Penicillium brasilianum* KUEB15 using statistical method. *J Ind Eng Chem* 25:145–150
- Kajani AA, Bordbar A-K (2019) Biogenic magnetite nanoparticles: a potent and environmentally benign agent for

- efficient removal of azo dyes and phenolic contaminants from water. *J Hazard Mater* 366:268–274
- Kalsoon R, Ahmed S, Nadeem M, Chohan S, Abid M (2019) Biosynthesis and extraction of cellulase produced by *Trichoderma* on agro-wastes. *Int J Environ Sci Technol* 16:921–928
- Karri RR, Tanzifi M, Yarak MT, Sahu J (2018) Optimization and modeling of methyl orange adsorption onto polyaniline nano-adsorbent through response surface methodology and differential evolution embedded neural network. *J Environ Manage* 223:517–529
- Katepetch C, Rujiravanit R (2011) Synthesis of magnetic nanoparticle into bacterial cellulose matrix by ammonia gas-enhancing in situ co-precipitation method. *Carbohydr Polym* 86:162–170
- Khan H, Kadam A, Dutt D (2020) Studies on bacterial cellulose produced by a novel strain of *Lactobacillus* genus. *Carbohydr Polym* 229:115513
- Kim J-H, Han K-A (2022) Optimization of bacterial cellulose production from alcohol lees by intermittent feeding strategy. *Braz J Chem Eng* 23:1–10
- Kuo C-H, Huang C-Y, Shieh C-J, Wang H-MD, Tseng C-Y (2019) Hydrolysis of orange peel with cellulase and pectinase to produce bacterial cellulose using *Gluconacetobacter xylinus*. *Waste Biomass Valoriz* 10:85–93
- Li J, Shi S, Wang Y, Jiang Z (2021) Integrated production of optically pure L-lactic acid from paper mill sludge by simultaneous saccharification and co-fermentation (SSCF). *Waste Manag* 129:35–46
- Lin S-P, Huang S-H, Ting Y, Hsu H-Y, Cheng K-C (2022) Evaluation of detoxified sugarcane bagasse hydrolysate by atmospheric cold plasma for bacterial cellulose production. *Int J Bio Macromol* 204:136–143
- Lisdiyanti P, Suyanto E, Gusmawati NF, Rahayu W (2012) Isolation and characterization of cellulase produced by cellulolytic bacteria from peat soil of Ogan Komering Ilir. *South Sumat Int J Environ Bioenerg* 3:145–153
- Liu F, Chen C, Qian J (2021) Film-like bacterial cellulose/cyclodextrin oligomer composites with controllable structure for the removal of various persistent organic pollutants from water. *J Hazard Mater* 405:124122
- Ludwig TG, Goldberg HJ (1956) The anthrone method for the determination of carbohydrates in foods and in oral rinsing. *J Dent Res* 35:90–94
- Mais U, Esteghlalian AR, Saddler JN, Mansfield SD (2002) Enhancing the enzymatic hydrolysis of cellulosic materials using simultaneous ball milling. In: Mais U (ed) *Biotechnology for fuels and chemicals*. Springer, Singapore, pp 815–832
- Malik WA, Khan HM, Javed S (2022) Bioprocess optimization for enhanced production of bacterial cellulase and hydrolysis of sugarcane bagasse. *Bio Energy Res* 15:1116–1129
- Miller GL (1959) Use of dinitrosalicylic acid reagent for determination of reducing sugar. *Anal Chem* 31:426–428
- Mokale Kognou AL, Chio C, Khatiwada JR, Shrestha S, Chen X, Han S, Li H, Jiang Z-H, Xu CC, Qin W (2022) Characterization of cellulose-degrading bacteria isolated from soil and the optimization of their culture conditions for cellulase production. *Appl Biochem Biotechnol* 194:5060–5082
- Muzenda C, Arotiba OA (2022) Improved magnetite nanoparticle immobilization on a carbon felt cathode in the heterogeneous electro-fenton degradation of aspirin in wastewater. *ACS Omega*, Washington
- Nathan VK, Esther Rani M, Rathinasamy G, Dhiraviam KN, Jayavel S (2014) Process optimization and production kinetics for cellulase production by *Trichoderma viride* VKF3. *Springerplus* 3:1–12
- Naves FL, de Paula TI, Balestrassi PP, Braga WLM, Sawhney RS, de Paiva AP (2017) Multivariate normal boundary intersection based on rotated factor scores: a multiobjective optimization method for methyl orange treatment. *J Clean Prod* 143:413–439
- Nguyen CH, Fu C-C, Juang R-S (2018) Degradation of methylene blue and methyl orange by palladium-doped TiO₂ photocatalysis for water reuse: Efficiency and degradation pathways. *J Clean Prod* 202:413–427
- Nidheesh P, Gandhimathi R, Velmathi S, Sanjini N (2014) Magnetite as a heterogeneous electro Fenton catalyst for the removal of Rhodamine B from aqueous solution. *RSC Adv* 4:5698–5708
- Ningthoujam R, Dhingra H (2022) Production of hydrolytic cellulase enzyme by isolate *Aspergillus flavus* OR and *Trichoderma reesei* using rice straw as the feedstock material. *Annal Agri Bio Res* 27:8–11
- Otani H, Udway DW, Mouncey NJ (2022) Comparative and pangenomic analysis of the genus *Streptomyces*. *Sci Rep* 12:18909
- Padmanabhan SK, Lionetto F, Nisi R, Stoppa M, Licciulli A (2022) Sustainable production of stiff and crystalline bacterial cellulose from orange peel extract. *Sustain* 14:2247
- Perwez M, Fatima H, Arshad M, Meena V, Ahmad B (2022) Magnetic iron oxide nanosorbents effective in dye removal. *Int J Environ Sci Technol* 32:1–18
- Pham VHT, Kim J, Shim J, Chang S, Chung W (2022) Coconut mesocarp-based lignocellulosic waste as a substrate for cellulase production from high promising multi-enzyme-producing *Bacillus amyloliquefaciens* FW2 without pretreatments. *Microorganisms* 10:327
- Premalatha N, Gopal NO, Jose PA, Anandham R, Kwon S-W (2015) Optimization of cellulase production by *Enhydrobacter* sp ACCA2 and its application in biomass saccharification. *Front Microbiol* 6:1046
- Saini R, Saini JK, Adsul M, Patel AK, Mathur A, Tuli D, Singhania RR (2015) Enhanced cellulase production by *Penicillium oxalicum* for bio-ethanol application. *Bioresour Technol* 188:240–246
- Saini K, Sahoo A, Biswas B, Kumar A, Bhaskar T (2021) Preparation and characterization of lignin-derived hard templated carbon (s): statistical optimization and methyl orange adsorption isotherm studies. *Bioresour Technol* 342:125924
- Salama A, Etri S, Mohamed SA, El-Sakhawy M (2018) Carboxymethyl cellulose prepared from mesquite tree: New source for promising nanocomposite materials. *Carbohydr Polym* 189:138–144
- Saleh AK, Soliman NA, Farrag AA, Ibrahim MM, El-Shinawy NA, Abdel-Fattah YR (2020) Statistical optimization and characterization of a biocellulose produced

- by local Egyptian isolate *Komagataeibacter hansenii* AS. 5. *Int J Biol Macromol* 144:198–207
- Saleh AK, El-Gendi H, Ray JB, Taha TH (2021) A low-cost effective media from starch kitchen waste for bacterial cellulose production and its application as simultaneous absorbance for methylene blue dye removal. *Biomass Convers. Biorefin* 12:1–13
- Saleh AK, Abdel-Fattah YR, Soliman NA, Ibrahim MM, El-Sayed MH, Abd El-Aziz ZK, El-Zawawy WK (2022a) Box-Behnken design for the optimization of bioethanol production from rice straw and sugarcane bagasse by newly isolated *Pichia occidentalis* strain AS. 2. *Energy Environ* 33:1613–1635
- Saleh AK, El-Gendi H, El-Fakharany EM, Owda ME, Awad MA, Kamoun EA (2022b) Exploitation of cantaloupe peels for bacterial cellulose production and functionalization with green synthesized Copper oxide nanoparticles for diverse biological applications. *Sci Rep* 12:19241
- Saleh AK, El-Gendi H, Soliman NA, El-Zawawy WK, Abdel-Fattah YR (2022c) Bioprocess development for bacterial cellulose biosynthesis by novel *Lactiplantibacillus plantarum* isolate along with characterization and antimicrobial assessment of fabricated membrane. *Sci Rep* 12:1–17
- Saratale GD, Saratale RG, Oh SE (2012) Production and characterization of multiple cellulolytic enzymes by isolated *Streptomyces* sp. *MDS Biomass Bioenergy* 47:302–315
- Segal L, Creely JJ, Martin AE, Conrad CM (1959) An empirical method for estimating the degree of crystallinity of native cellulose using the X-ray diffractometer. *Text Res J* 29(10):786–794.
- Sharma C, Bhardwaj NK, Pathak P (2021) Static intermittent fed-batch production of bacterial nanocellulose from black tea and its modification using chitosan to develop antibacterial green packaging material. *J Clean Prod* 279:123608
- Shezad O, Khan S, Khan T, Park JK (2010) Physicochemical and mechanical characterization of bacterial cellulose produced with an excellent productivity in static conditions using a simple fed-batch cultivation strategy. *Carbohydr Polym* 82:173–180
- Shirling ET, Gottlieb D (1966) Methods for characterization of *Streptomyces* species. *Int J Syst Bacteriol* 16:313–340
- Siqueira JGW, Rodrigues C, de Souza VLP, Woiciechowski AL, Soccol CR (2020) Current advances in on-site cellulase production and application on lignocellulosic biomass conversion to biofuels: a review. *Biomass Bioenergy* 132:105419
- Song W, Li J, Zhang X, Feng J, Du X, Wang Q, Fu C, Qiu W, Wang Z, Gao X (2022) A feasible approach for azo-dye methyl orange degradation in siderite/H₂O₂ assisted by persulfate: Optimization using response surface methodology and pathway. *J Environ Manage* 308:114397
- Srivastava N, Singh R, Srivastava M, Syed A, Pal DB, Bahkali AH, Mishra P, Gupta VK (2022) Impact of mixed lignocellulosic substrate and fungal consortia to enhance cellulase production and its application in NiFe₂O₄ nanoparticles mediated enzymatic hydrolysis of wheat straw. *Bioresour Technol* 345:126560
- Strezov V, Evans TJ (2009) Thermal processing of paper sludge and characterisation of its pyrolysis products. *Waste Manage* 29:1644–1648
- Sulaeva I, Hettegger H, Bergen A, Rohrer C, Kostic M, Konnerth J, Rosenau T, Potthast A (2020) Fabrication of bacterial cellulose-based wound dressings with improved performance by impregnation with alginate. *Mater Sci Eng C* 110:110619
- Surip S, Abdulhameed AS, Garba ZN, Syed-Hassan SSA, Ismail K, Jawad AH (2020) H₂SO₄-treated Malaysian low rank coal for methylene blue dye decolourization and cod reduction: optimization of adsorption and mechanism study. *Surf Interfaces* 21:100641
- Tahari N, de Hoyos-Martinez PL, Izaguirre N, Houwaida N, Abderrabba M, Ayadi S, Labidi J (2022) Preparation of chitosan/tannin and montmorillonite films as adsorbents for Methyl Orange dye removal. *Int J Biol Macromol* 210:94–106
- Takizawa S, Baba Y, Tada C, Fukuda Y, Nakai Y (2018) Pretreatment with rumen fluid improves methane production in the anaerobic digestion of paper sludge. *Waste Manag* 78:379–384
- Tamer Y, Özeren MD, Berber H (2021) High adsorption performance of graphene oxide doped double network hydrogels for removal of azo dyes from water and their kinetics. *J Polym Environ* 29:4000–4016
- Tanhaei B, Ayati A, Lahtinen M, Sillanpää M (2015) Preparation and characterization of a novel chitosan/Al₂O₃/magnetite nanoparticles composite adsorbent for kinetic, thermodynamic and isotherm studies of Methyl Orange adsorption. *Chem Eng J* 259:1–10
- Tapias YAR, Di Monte MV, Peltzer MA, Salvay AG (2022) Bacterial cellulose films production by Kombucha symbiotic community cultured on different herbal infusions. *Food Chem* 372:131346
- TAPPI (1983) TAPPI T222 om-83. Acid-insoluble lignin in wood and pulp, TAPPI Testing Procedures, Atlant
- TAPPI (1984) Moisture in wood, pulp, paperboard by toluene distillation. TAPPI testing procedures, Atlanta
- TAPPI (1985) TAPPI T257 om-85. Sampling and preparing wood for analysis. TAPPI testing procedures, Atlanta
- TAPPI (1993) TAPPI T211 om-93. Stander test methods for forming handsheets for physical test pulp, TAPPI testing procedures, Atlanta
- Taramian A, Doosthoseini K, Mirshokraii SA, Faezipour M (2007) Particleboard manufacturing: an innovative way to recycle paper sludge. *Waste Manag* 27:1739–1746
- Tripathi M, Sharma M, Bala S, Connell J, Newbold JR, Rees RM, Aminabhavi TM, Thakur VK, Gupta VK (2023a) Conversion technologies for valorization of hemp lignocellulosic biomass for potential biorefinery applications. *Sep Purif Technol* 320:124018
- Tripathi M, Singh P, Singh R, Bala S, Pathak N, Singh S, Chauhan RS, Singh PK (2023b) Microbial biosorbent for remediation of dyes and heavy metals pollution: a green strategy for sustainable environment. *Front Microbiol* 14:1168954
- Turner T, Wheeler R, Oliver IW (2022) Evaluating land application of pulp and paper mill sludge: a review. *J Environ Manage* 317:115439

- Usmani Z, Sharma M, Diwan D, Tripathi M, Whale E, Jayakody LN, Moreau B, Thakur VK, Tuohy M, Gupta VK (2022) Valorization of sugar beet pulp to value-added products: a review. *Bioresour Technol* 346:126580
- Wang C-H, Hseu T-H, Huang C-M (1988) Induction of cellulase by cello-oligosaccharides in *Trichoderma koningii* G-39. *J Biotechnol* 9:47–59
- Wang L, Mao L, Qi F, Li X, Ullah MW, Zhao M, Shi Z, Yang G (2021a) Synergistic effect of highly aligned bacterial cellulose/gelatin membranes and electrical stimulation on directional cell migration for accelerated wound healing. *Chem Eng J* 424:130563
- Wang Q, Nnanna PC, Shen F, Huang M, Tian D, Hu J, Zeng Y, Yang G, Deng S (2021b) Full utilization of sweet sorghum for bacterial cellulose production: a concept of material crop. *Ind Crops Prod* 162:113256
- Yang J, Yu J, Fan J, Sun D, Tang W, Yang X (2011) Biotemplated preparation of CdS nanoparticles/bacterial cellulose hybrid nanofibers for photocatalysis application. *J Hazard Mater* 189:377–383
- Yang C, Luo H, Cheng W, Jiang K, Lu L, Ling L (2022) Decolorization characteristics and mechanism of methyl orange dye by using *Stenotrophomonas acidaminiphila* EFS1. *Int J Environ Sci Technol* 63:1–10
- Zhang W, Tang G, Yan J, Zhao L, Zhou X, Wang H, Feng Y, Guo Y, Wu J, Chen W (2020) The decolorization of methyl orange by persulfate activated with natural vanadium-titanium magnetite. *Appl Surf Sci* 509:144886
- Zhao P, Zhao Y, Guo Y, Guo R, Tian Y, Zhao W (2021) Preparation of CuO/ γ -Al₂O₃ catalyst for degradation of azo dyes (reactive brilliant red X-3B): an optimization study. *J Clean Prod* 328:129624

Publisher's Note Springer Nature remains neutral with regard to jurisdictional claims in published maps and institutional affiliations.